Calderas

5

5.1 Introduction

After having described magma chamber formation and growth in Chap. 4, this fifth chapter considers the surface processes resulting from the dynamics of magma chambers, including magma accumulation on the long- and short-term, and rapid magma withdrawal and eruption. The rapid withdrawal of magma may develop a caldera. Calderas often represent the surface expression of long-lived and large magmatic reservoirs, which may be responsible for the most destructive eruptions. Calderas are active on different time scales as, in addition to experiencing eruptions and collapse (lasting from days to weeks), also experience degassing, seismicity and surface deformation testifying unrest (from months to decades), eventually culminating in long-term uplift, or resurgence (from hundreds to thousands of years). Commonly lacking a central conduit, calderas may be associated with eruptive vents scattered over a wide area, posing a higher risk than central volcanoes. Finally, calderas may also provide resources, through geothermal and ore deposits exploitation.

Calderas thus constitute an end-member type of volcano, providing the most challenging yet exciting ground for volcanologists.

The main aims of this chapter are to:

- describe the structure and evolution of calderas, including the nature of their ring faults;
- discuss resurgence, resulting from long-term magma accumulation, and its mechanisms;
- introduce caldera unrest, resulting from short-term magma accumulation, and discuss its relations to resurgence;
- discuss how the caldera structure controls the transfer of the magma accumulated below, eventually feeding eruptions at different locations.

5.2 General Features of Calderas

Calderas are subcircular depressions in volcanic areas, with diameter between approximately one and several tens of kilometres (Fig. 5.1). Caldera formation is associated with the withdrawal of magma from an underlying chamber; the withdrawal induces the foundering of the chamber roof, determining the depression at the surface. The withdrawal may result from the rise and eruption, at times with explosive behaviour and significant size, of magma from the chamber. Alternatively, calderas may result from the lateral intrusion of magma through a dike or sill, eventually feeding a minor to moderate distal effusive eruption. Therefore, calderas may be associated with effusive or explosive eruptions of any size (Druitt and Sparks 1984; Branney and Acocella 2015).

The original version of this chapter was revised: Fig. 5.13 has been corrected. The correction to this chapter is available at https://doi.org/10.1007/978-3-030-65968-4_14

V. Acocella, *Volcano-Tectonic Processes*, Advances in Volcanology,
https://doi.org/10.1007/978-3-030-65968-4_5

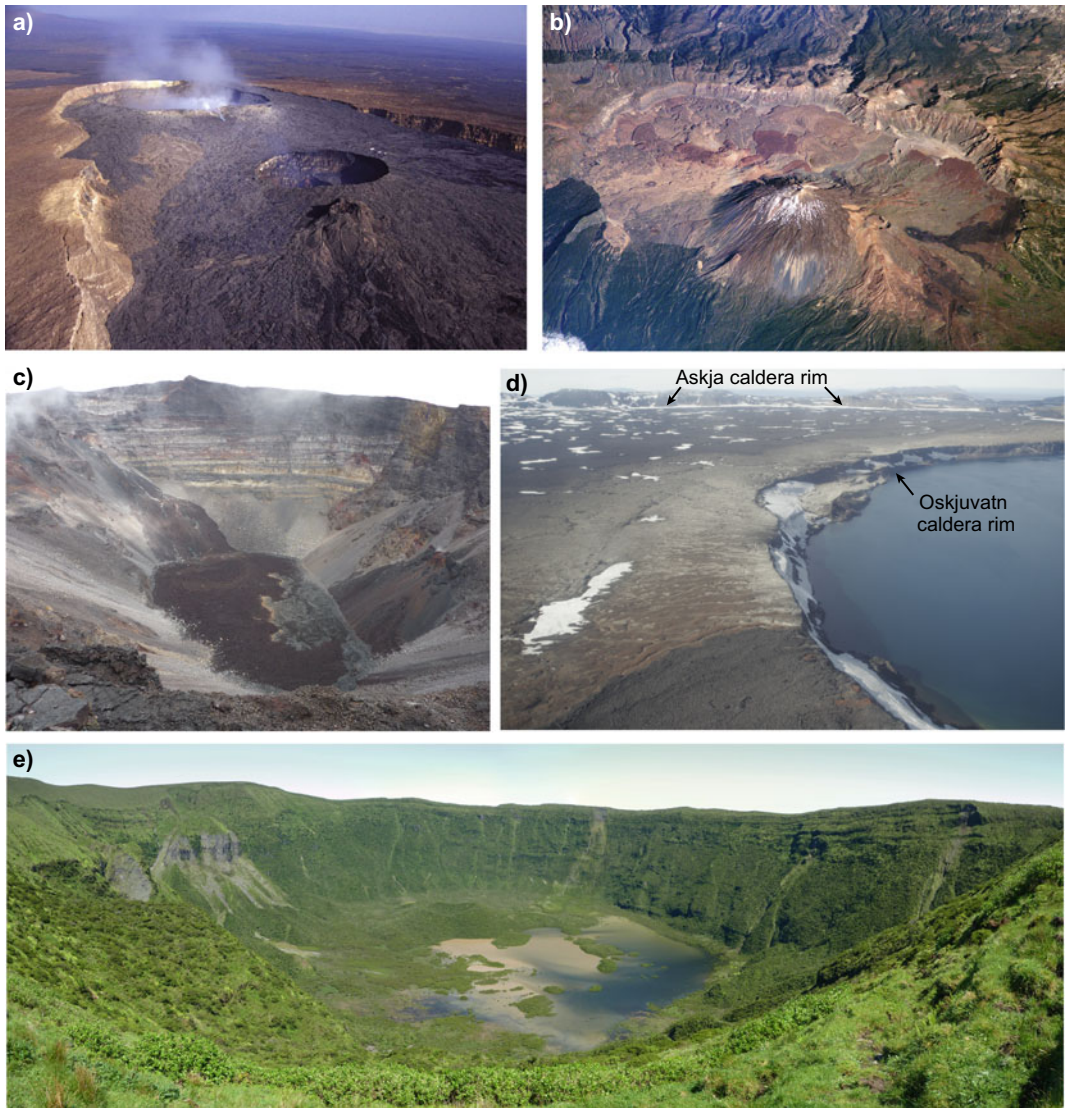

Fig. 5.1 Views of different calderas. **a** Erta Ale caldera, Afar, Ethiopia, hosting two pit craters. **b** Las Canadas caldera, Tenerife (Canary Islands), as seen from the International Space Station on June 6, 2006; the stratovolcano on the caldera rim in the foreground is Pico de Teide, 3715 m high; image property NASA. **c** Dolomieu caldera (Piton de la Fournaise, La Reunion Island), formed in April 2007. **d** Western rim of the 1875 Öskjuvatn caldera (Iceland), filled by the lake, nested within the larger and older Askja caldera, whose rim is visible in the background (see also Fig. 5.4b). **e** Caldera of the Caldeira stratovolcano on Faial, Azores

The most distinctive feature of a caldera consists of one or more ring faults, usually arcuate in map view, along which the roof of the chamber collapses. The **ring fault** separates an outer non-collapsed zone from an inner collapsed zone, thus representing the caldera **structural boundary** (Fig. 5.2). The ring fault forms during caldera collapse, but it may be soon intruded by the magma, generating a ring-dike ultimately feeding eruptive vents (see Sect. 7.5.3). In particular, the ring fault propagates upward from the chamber upon magma withdrawal. If the amount

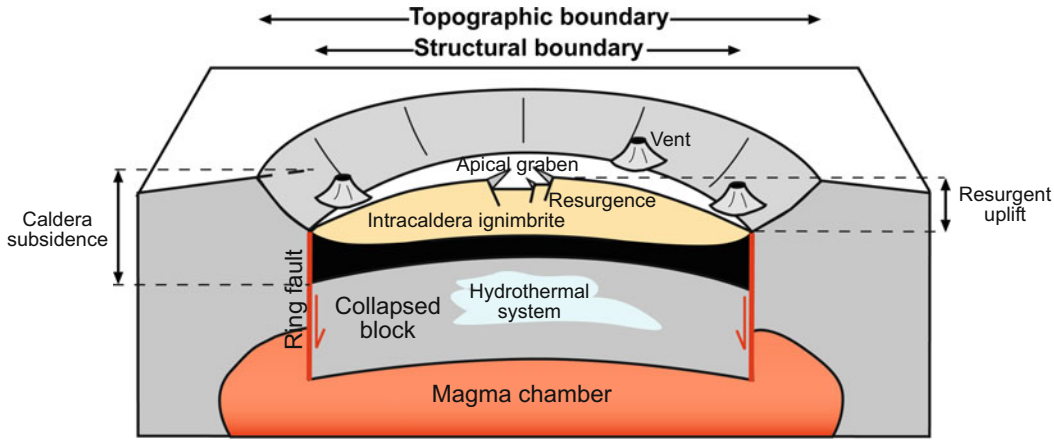

Fig. 5.2 Main morphological, structural and magmatic features of a caldera; not to scale (modified after Cole et al. 2005)

of subsidence of the caldera is significant, the ring fault may carry an important displacement and reach the surface. However, massive erosion during and after caldera collapse usually prevents observing a pristine ring fault, leaving an erosional scarp highlighted by a steep slope: this is the caldera **topographic boundary**, which may be as high as one kilometre (Lipman 1997; Cole et al. 2005). Because of retrogressive erosion, the topographic boundary lies externally to the structural boundary. Conversely, if the amount of subsidence is not significant, the ring fault may not reach the surface and a broad flexure, or monocline, forms above it; in this case, the downsag-like caldera boundary lacks a topographic scarp.

The caldera depression may be filled with volcanic deposits (including any intra-caldera ignimbrite), landslide breccia from the structural and topographic boundaries, and deposits deriving from any water infill (sea, lake, groundwater). The amount of subsidence of the caldera results from the difference in elevation of a known pre- or syn-collapse marker outside and within the caldera. However, any post-collapse vertical motion may significantly displace the caldera floor. This is the case of **resurgence**, consisting of a significant (tens of metres at least) and prolonged (hundreds of years at least) uplift of the caldera floor, highlighted by the anomalous height of its infill, accompanied by doming and/or faulting (see Sect. 5.6). A **hydrothermal system** commonly lies between the caldera floor and the magma chamber, focusing at depths between ~1 and ~4 km; here meteoric and magmatic fluids are pressurized within a fracture network that increases permeability (e.g., Garden et al. 2020).

These basic ingredients may be complicated by several factors, leading to elongated, overlapping, nested and asymmetric collapses. Elongated collapses are elliptical in map view and usually result from the activity of a regional stress field (see Sect. 5.5), as at Long Valley caldera (California, USA). In a few cases, elongated collapses may result from aligned overlapping calderas due to reservoir withdrawal along a same direction, as Las Canadas (Tenerife, Canary Islands; Fig. 5.1b). Nested calderas consist of one collapse structure within the other and may be related to a pair of eruptions or the same eruptive event (see Sect. 5.3). Asymmetric (or trapdoor) collapses are common, with one side subsided much more than the opposite. These result from asymmetries in the magma chamber shape, in the withdrawal of magma from the chamber, or from the drag effect reducing resistance along the foundering block within a molten chamber (Marti and Gudmundsson 2000; Acocella 2007; Kennedy et al. 2008).

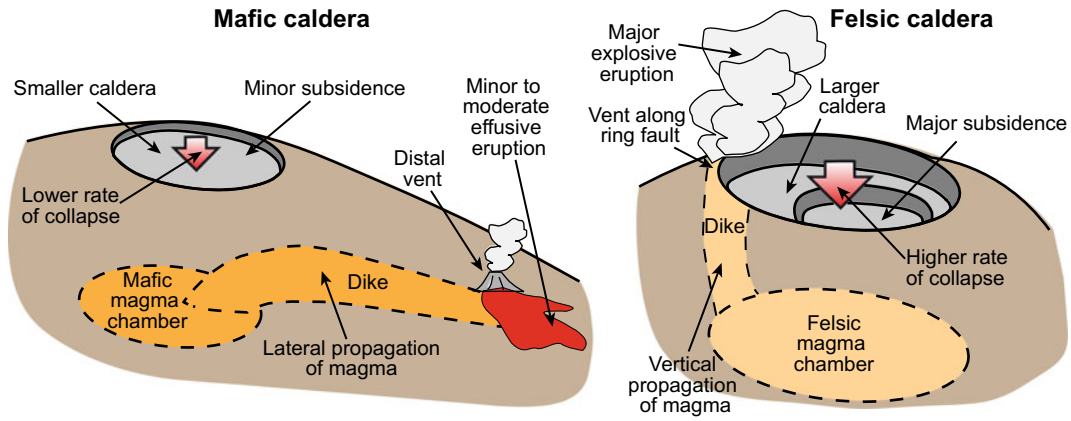

Fig. 5.3 Recurrent features commonly associated with mafic (left) and felsic (right) calderas; not to scale

Generally there is a broad relationship among the amount (from a few tens of metres to a very few kilometres) and rate (from cm/day to km/day) of collapse of calderas, the mechanism of magma withdrawal (lateral intrusion with effusive eruption, or vertical intrusion with explosive eruption), the size (from 10^{-1} to 10^{3} km^{3}) and the composition (mafic or felsic) of the involved magma (Fig. 5.3; Newhall and Dzurisin 1988; Branney and Acocella 2015). Minor effusive eruptions often occur in the distal portion of smaller mafic calderas subsiding moderately (tens to hundreds of m) over longer periods (days to months); these calderas and eruptions are usually associated with the lateral intrusion of mafic magma. Conversely, major explosive summit eruptions are often related to felsic calderas formed in shorter time spans (hours to days) with significant subsidence (up to a very few kilometres); these calderas and eruptions are related to the vertical propagation and eruption of felsic magma. These general, but not unique, features suggest that ultimately the composition of the involved magma, related to the size of the system, controls the type and location of the eruption, as well as the rate of magma withdrawal and the amount of subsidence. Based on this, it is useful to further distinguish between the behaviour of mafic and felsic calderas.

Mafic calderas usually occur on shield volcanoes and erupt predominantly basaltic magma, although more evolved compositions (up to rhyolites) may be also erupted. These calderas are commonly up to several kilometres wide, with total amount of subsidence of a few hundred of metres, achieved with rates from cm/day to m/day. These mafic calderas may consist of smaller and structurally simpler systems, as Kilauea and Mauna Loa (Hawaii, USA), Piton de la Fournaise (La Réunion) and Erta Ale (Afar, Ethiopia), or larger and structurally more complex systems, as Askja (Iceland), Fernandina and Sierra Negra (Galapagos) (Fig. 5.4). The smaller and structurally simpler calderas usually show a moderate amount of collapse along a single subcircular ring fault, whose topographic expression consists of a hundred metres high subvertical scarp on a pile of lava flows. Extension fractures, up to a few metres wide, form in the upper portion (head) of the subvertical scarp zone and parallel to this, as induced by the lack of confinement created by the scarp. The fractures bound unstable blocks which eventually topple in the caldera, promoting the erosional retreat of the scarp. These calderas are commonly associated with distal effusive eruptions resulting from the lateral intrusion of magma through dikes (see Sect. 5.10.3). Mafic calderas may be also wider and structurally more complex (for example showing nested depressions), with higher subsidence associated with larger and more explosive eruptions, occurring also within the caldera itself. This type of calderas are

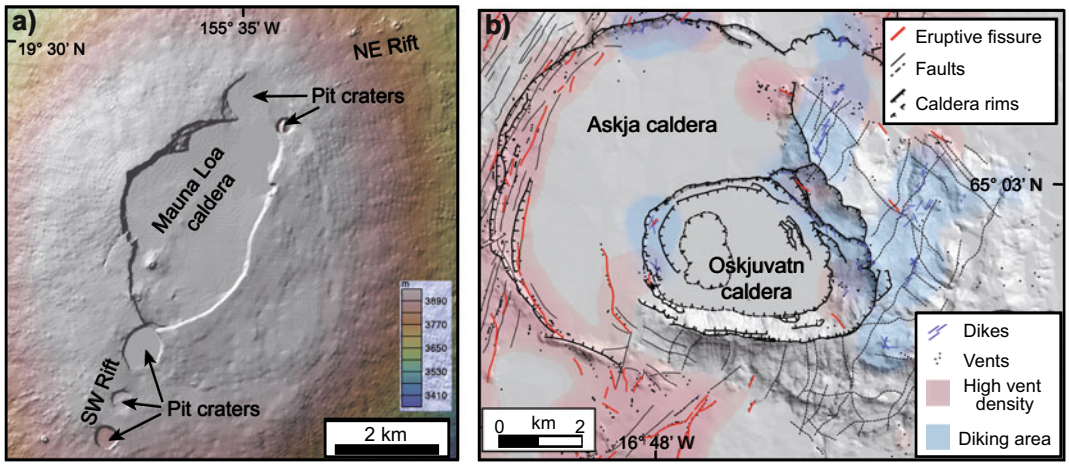

Fig. 5.4 Examples of mafic calderas. **a** Digital elevation model of Mauna Loa caldera (Hawaii, USA), showing the main caldera and the pit craters along the volcanic rift zones departing from the volcano summit (base from GeoMapApp). **b** Map view structure of the more complex nested caldera of Askja, Iceland, showing the larger Askja and the younger (formed in 1875) Oskjuvatn calderas (modified after Trippanera et al. 2018)

relatively common in the western Galapagos Islands, where the steeper summit of the shield-like volcanic edifice, resembling an "overturned soup plate", also hosts distinctive circumferential eruptive fissures (see Sect. 7.5; Chadwick and Howard 1991).

Smaller-scale analogues of mafic calderas, as sharing magma withdrawal at depth, are **pit craters,** which are metres to hundreds of metres wide subcircular depressions found along volcanic rift zones, whose formation is commonly related to the lateral flow and local stoping of magma along dikes. Pit craters are often associated with calderas, occurring within (as at Erta Ale or Kilauea) or to the side of the caldera (as at Mauna Loa and Piton de la Fournaise). The eroded Nindiri and Santiago pit craters at Masaya (Nicaragua), a few hundred of metres wide and several tens of metres deep, offer the rare opportunity to observe their deeper structure, consisting of concentric reverse (inner) and normal (outer) faults (Okubo and Martel 1998; Rymer et al. 1998; Harris 2009)

Felsic calderas are frequently associated with the explosive eruption of evolved magma and show greater variability in size, structure and activity, and often experience resurgence. Their width can reach several tens of kilometres, whereas the amount of subsidence a few kilometres, with subsidence rates of km/day. Being able to accumulate magma and generate major eruptions, felsic magma reservoirs below calderas are often large and long-lived. The true spatial extent of the felsic magma chambers may not be reflected by the size of their calderas. In fact, caldera size may be affected by the rheology of crystal-rich felsic magma, behaving elastically along the periphery of the chamber and developing calderas before complete remobilization of the entire reservoir. This may for example explain the magma chamber wider (90 km wide) than the caldera (60 km wide) at Yellowstone (Wyoming, USA; Karlstrom et al. 2012; Farrell et al. 2014).

The architecture of felsic calderas may consist of a single, major ring fault system accommodating subsidence (as Gariboldi, Ethiopia) or, more often, of pairs of nested concentric collapses, as Campi Flegrei and Latera (Italy), Guayabo (Costa Rica), La Pacana (Chile) or Taupo (New Zealand; Acocella 2007; Delgado and Pavez 2015). Many of these pairs of nested collapses are activated during the same eruptive event, not necessarily requiring two distinct eruptions, as at Campi Flegrei, where both the outer and inner collapses formed during

the ~39 ka Campania Ignimbrite eruption and were reactivated during the ~15 ka Neapolitan Yellow Tuff eruption. The deposits along the topographic boundary of felsic calderas usually consist of the proximal portions of the erupted caldera ignimbrites. These deposits are then easily eroded, promoting the departure of the topographic boundary from the structural boundary. If the subsidence is partitioned along several parallel ring faults, each carrying only a part of the displacement, these may better resist erosion; this is observed along the well-preserved eastern margin of Bolsena caldera (Italy), characterized by staircase faulting, conversely to the poorly-preserved northern margin, where the single ring fault carrying the subsidence experienced stronger erosion (Acocella et al. 2012).

Felsic systems also form the largest calderas (super-calderas) on Earth, with diameter of several tens of kilometres, such as Yellowstone and Toba (Sumatra, Indonesia). The Yellowstone volcanic field was formed during three major caldera-forming eruptions at ~2.05, ~1.3, and ~0.64 Ma, erupting ~2500 km^3, ~280 km^3 and ~1000 km^3 of magma, respectively (see Sect. 13.8). The youngest caldera-forming eruption generated the current caldera, followed by ~50 rhyolitic and basaltic events, the youngest at ~70 ka. The 40 × 60 km wide caldera hosts two fractured resurgent domes. Monitoring data indicate a restless behaviour, attributed to repeated intrusions of magma and/or the pressurization of the hydrothermal system by fluids released from more than 15,000 km^3 of rhyolitic magma at depths from 8 to 18 km, largely emplaced as sill complexes (Smith and Braile 1994; Christiansen 2001; Lowenstern et al. 2006; Chang et al. 2007; Jiang et al. 2018). Toba has been active in the past 1.3 Ma, producing the Earth's largest Quaternary eruption at ~75 ka, ejecting ~5300 km^3 DRE of magma. The 100 × 45 km caldera is NW–SE elongated, parallel to the nearby Great Sumatra Fault (Fig. 5.5; see Sect. 12.3.2). The caldera

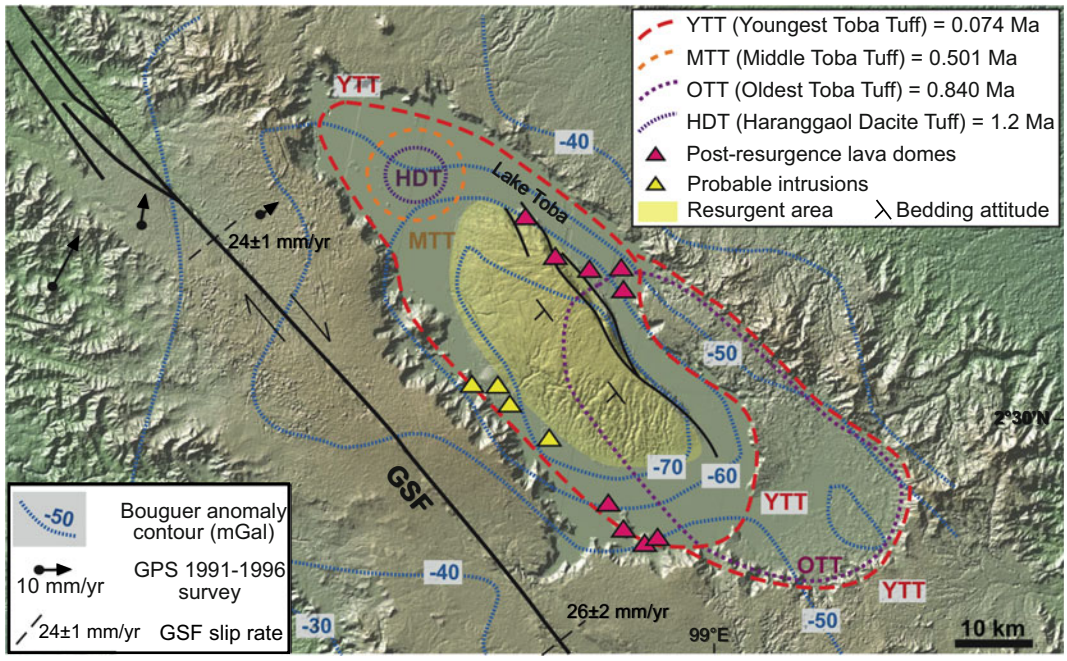

Fig. 5.5 Simplified structure of the large felsic caldera of Toba, Sumatra (Indonesia), including the collapses from the major eruptions, the resurgence area, the post-resurgence vents, the Bouguer anomalies and the slip rate along the Great Sumatra Fault (GSF; after Genrich et al. 2000; Masturyono et al. 2001; Chesner 2012; de Silva et al. 2015)

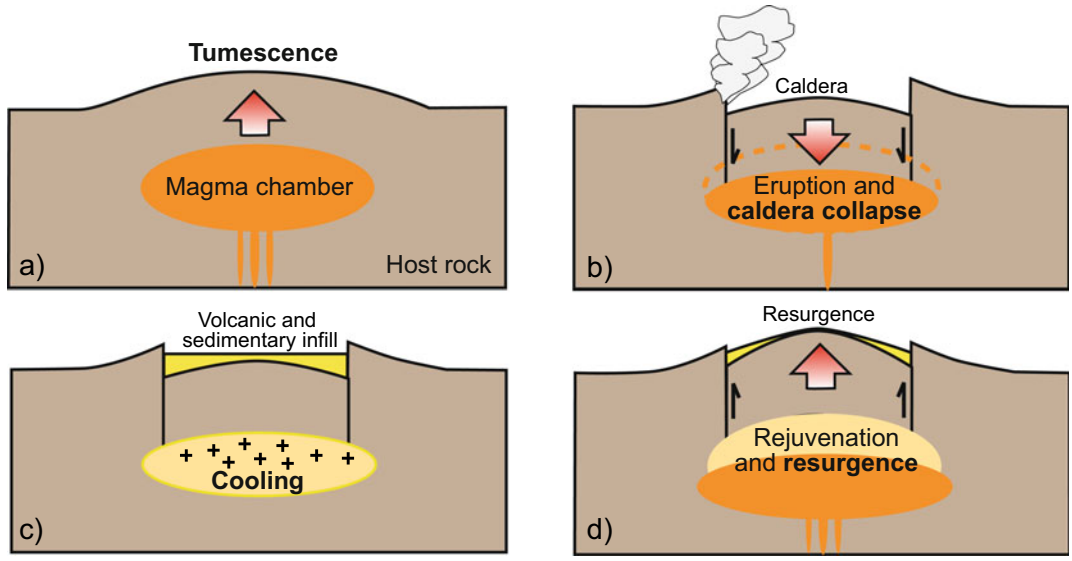

Fig. 5.6 Possible main evolutionary stages of a large felsic volcano with caldera: **a** initial tumescence, due to magma accumulation; **b** major eruption(s) and caldera formation; **c** evanescence and cooling of the shallow chamber; **d** rejuvenation, due to the input of new magma, promoting resurgence (modified after Smith and Bailey 1968)

hosts the NW–SE elongated Samosir resurgent block, uplifted asymmetrically of ~1100 m in less than 75 ka. Two nearby reservoirs, from 8 to 14 km depth, lie below the caldera (Vazquez and Reid 2004; Koulakov et al. 2009; Chesner 2012; de Silva et al. 2015; Solada et al. 2020).

An ideal evolution of large felsic magmatic complexes has been summarized in a few representative stages (Fig. 5.6; Smith and Bailey 1968; Lipman 1984). (a) Initial tumescence**,** due to prolonged magma emplacement inducing broad surface uplift. (b) One or more major eruptions, promoting caldera formation. (c) Decaying activity, when the mature magma chamber experiences discontinuous supply and faster cooling. (d) Possible resurgence, when new magma rejuvenates the shallow reservoir, uplifting the caldera floor.

5.3 Structure and Evolution

Despite recent episodes of caldera collapse, field and geophysical data provide limited access to understand the structure of calderas, in particular the resolution of the "space problem", that is how to accommodate the subsidence of the collapsed portion, which also determines the geometry and kinematics of the caldera's ring faults. To this aim, analogue, analytical and numerical models have been performed, providing insights on the architecture and development of calderas (e.g., Geyer and Martì 2014).

All analogue models have shown that, independently of the different boundary conditions, the structure of a caldera is mainly a function of its amount of subsidence (Fig. 5.7; Acocella 2007). For minor subsidence, the upward propagating ring fault does not reach the surface and thus a flexure forms above the blind ring fault (Stage 1). Increasing the subsidence, the ring fault reaches the surface, replacing the flexure with a fault scarp (Stage 2). The fault is outward dipping with reverse kinematics, which results from the differential vertical motion between the two blocks, responsible for a deflection of the maximum principal stress σ_1 from the vertical path. Therefore, these reverse faults are not related to any lateral compression (see detail of σ_1 trajectories in stage 2, Fig. 5.7; Mandl 1988). An increase in subsidence produces a peripheral flexure, resulting from the upward propagation of

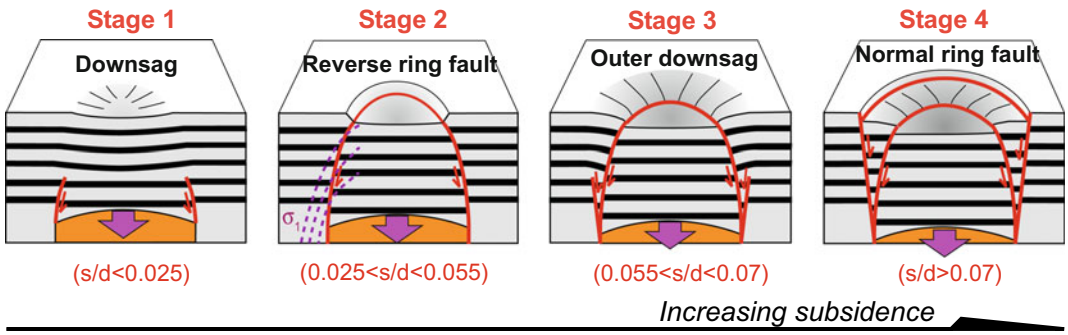

Fig. 5.7 The four evolutionary stages of caldera collapse, depending upon the *s*/*d* ratio, obtained in the analogue models and observed in nature. Stage 1: downsag; stage 2: reverse ring fault (dashed purple lines illustrate local configuration of the σ_1 trajectories controlling the development of the reverse fault); stage 3: peripheral downsag; stage 4: peripheral normal ring fault (modified after Acocella 2007)

an outer blind ring fault, driven by the gravitational collapse of the unstable wedge of the hanging wall of the reverse ring fault (Stage 3). In the final stage, increasing again the subsidence, the outer ring fault reaches the surface, producing a second peripheral and concentric scarp, or nested collapse (Stage 4). This outer fault is inward dipping and has a normal kinematics due to the collapse of the wedge above the reverse fault. Any further increase in subsidence does not change this deformation pattern and both ring faults continue to be active.

These results, being obtained by independent studies under different boundary conditions, provide a robust platform to define the structure of calderas as a function of the amount of subsidence. However, calderas with different diameter may show different structures (corresponding to the above-mentioned evolutionary stages) even with similar amount of subsidence. For example, the same amount of subsidence may produce immature (stage 1) collapse in wider calderas or mature (stage 4) collapse in narrower calderas. This results from the fact that a same amount of subsidence in wider calderas develops a wider flexure accumulating larger vertical displacement before faulting. Therefore, to compare the structure and evolutionary stage of calderas, it is important to relate the amount of subsidence *s* to the caldera diameter *d*, that is considering the *s*/*d* ratio.

A second-order parameter controlling caldera structure is the depth to the magma chamber with regard to its width. For a given magma chamber width, shallower chambers produce the simple pattern described in Fig. 5.7, whereas deeper chambers promote multiple sets (whose number increases with the chamber depth) of overlapping outward dipping reverse ring faults, and only an uppermost normal ring fault (Roche et al. 2000). Often the entire collapse structure above these deep and narrow magma chambers is slightly inclined, forming a "sliding-trapdoor", or ring-fault architecture that consists of outward-inclined reverse portions and inward-inclined normal portions on opposite sides of the ring fault. This feature has been recognized at recent caldera collapses at Miyakejima (Japan), Dolomieu (Reunion) and Bardarbunga (Iceland; Bathke et al. 2015). However, in case of deep magma chamber with limited subsidence, the caldera faults may not reach the surface, delaying the expected evolutionary stages. Therefore, the deeper the magma chamber, the least developed is the collapse at the surface, as a larger amount of withdrawn magma is required to have collapse (Roche and Druitt 2001; Geyer et al. 2006). This feature has important implications in terms of magma transfer and eruption (see Sect. 5.9).

Analytical and numerical models of calderas provide less consistent results than analogue models, probably for the difficulty to simulate the

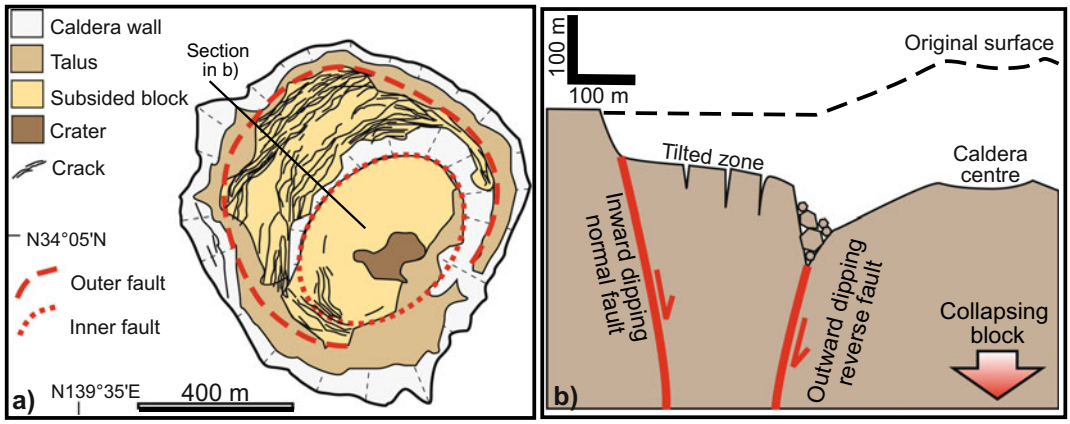

Fig. 5.8 Map (left) and section (right) views of Miyakejima caldera (Japan), as formed in 2000 (Japan; modified after Geshi et al. 2002). Compare with Fig. 5.7, stage 4

activity of shear fractures. In fact, only discrete element models in a frictional medium simulated caldera formation consistently with analogue models, developing upward propagating outward dipping reverse ring faults and peripheral inward dipping normal ring faults (Gudmundsson 2007; Hardy 2008; Holohan et al. 2011; Gregg et al. 2012; Kabele et al. 2017).

More importantly, the analogue modelling results are supported by geological and geophysical evidence from several tens of active mafic and felsic calderas, and direct observation of recent caldera collapses, in particular at Miyakejima, Axial Seamount and Kilauea (Fig. 5.8; Geshi et al. 2002; Acocella 2007; Wilcox et al. 2016; Levy et al. 2018; Baillard et al. 2019; Neal et al. 2019). This consistency indicates a robust frame to understand caldera structure and evolution, with the four stages allowing to define the overall structure of a caldera simply knowing its *s*/*d* ratio or, conversely, to define the amount of subsidence from the surface deformation pattern. Determining the *s*/*d* ratio of a caldera also allows classifying calderas (see Sect. 5.4) and better defining magma transfer below calderas, possibly forecasting the location of eruptive vents (see Sect. 5.9; Acocella and Rivalta 2019).

Kinematically, analogue models also show that collapse may occur with several modes and velocities (continuous, incremental or sudden), mainly depending on the aspect ratio (thickness/width) of the crust overlying the chamber and the reactivation of pre-existing ring faults. This feature is consistent with geophysical (mainly seismicity) and geodetic (mainly tilt variations) data from collapsing calderas (Michon et al. 2011; Ruch et al. 2012; Munekane et al. 2016). Also, models show that the propagation rates for the reverse faults during collapse increase with magma evacuation rates, with magma chamber dynamics and fault propagation being kinematically coupled (Seropian and Stix 2018). However, this relation may be influenced by the friction along the ring fault. For example, direct access to the ring fault of the extinct Jangsan caldera (Korea) reveals extremely low dynamic frictions, suggesting that an extraordinarily large fault slip (>100 m), causing a large earthquake, was associated with caldera formation. This slip generated pseudotachylytes, indicating that frictional melting was an important fault zone process during caldera collapse (Han et al. 2019; Kim et al. 2019).

5.4 Classification

A first popular approach to a systematic definition of caldera types was based on field data from active and extinct eroded calderas, defining five end-member geometries: piston, piecemeal,

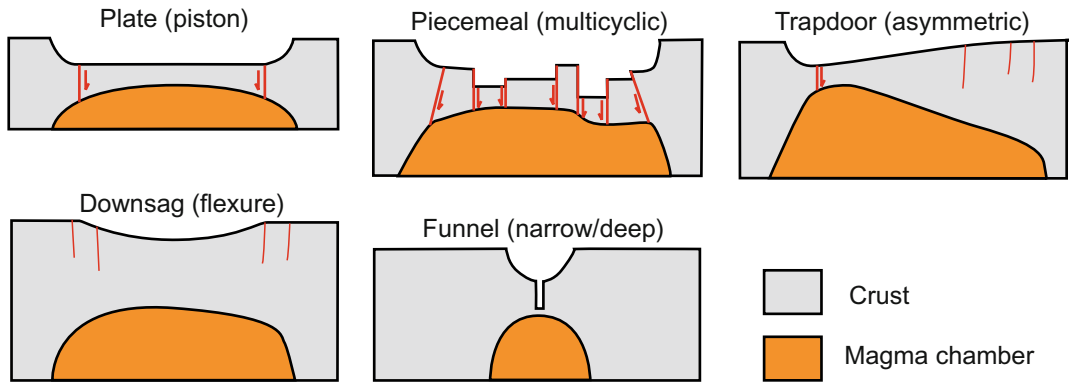

Fig. 5.9 The five established geometric caldera types (modified after Lipman 1997; Cole et al. 2005)

trapdoor, downsag and funnel (Fig. 5.9; Walker 1984; Lipman 1997, 2000; Cole et al. 2005). **Piston**-type calderas are bordered by a ring fault, delimiting a sinking central block. **Piecemeal** calderas result from the differential subsidence of multiple blocks, usually along several pre-existing faults. **Trapdoor** calderas show asymmetric subsidence accommodated by different types of structures along the rim, as a flexure on one side and a fault on the opposite. **Downsag** calderas are depressions with unfaulted and inward tilted, or flexured, margins. **Funnel** calderas are narrow and deep cone-shaped depressions.

While this geometric classification is based on easily detectable field features, justifying its popularity, it also carries several limitations concerning the structure and evolution of calderas. In particular: (a) this classification does not take into account for the resolution of the "space problem"; (b) this classification is based on a static perspective of calderas, not considering their development, maturity and possible evolutionary relationships; (c) several of the five proposed caldera types may be found within a same caldera, making it difficult to unequivocally capture its distinctive structure and evolutionary stage. For example, Bolsena caldera (Italy) contains a central piston collapsed asymmetrically, with one margin interpreted as a downsag and the other as a piecemeal (Acocella et al. 2012): accordingly, Bolsena should be awkwardly defined as a caldera with "trapdoor piston and downsagged and piecemeal margins".

The analogue models and their comparison to nature allow passing these limitations and proposing, using the s/d ratio of a caldera, a revised and more practical classification. As the shallow structure of calderas corresponds to a precise architecture at depth, recognizing diagnostic surface features allows a caldera to be categorized within a precise structural and evolutionary context. The general relationship between the evolutionary stages of a caldera and their range of s/d ratios explains the architecture and maturity of calderas along a continuum mainly controlled by progressive subsidence. In this context, stage 1 (downsag) calderas are characterized by $s/d < 0.025$, stage 2 (reverse fault) by $0.025 < s/d < 0.055$, stage 3 (outer downsag) by $0.055 < s/d < 0.07$ and stage 4 (normal fault) by $s/d > 0.07$ (Fig. 5.7; Acocella 2007). Using such a classification it is also possible to define the deeper structure of a caldera from the available surface evidence: the apparently complex structure of Bolsena would be simply explained by a stage 3 asymmetric collapse.

A more recent classification of calderas relies on the pressure variation inside the magma chamber with regard to eruption, considering underpressure and overpressure calderas (Martì et al. 2009). Underpressure calderas result from subsidence after decompression of the magma

chamber following a pre-caldera eruptive episode, according to the established model of caldera formation. Here the initiation of collapse is a consequence of the eruption, and this is expected to constitute the condition most frequently occurring in nature. However, in some cases there may be evidence that the stress conditions developing the caldera ring faults are achieved before the eruption. This is the theoretical rationale behind overpressure calderas, which may form when, for example, an overpressurized sill-like magma chamber is loaded by regional doming or undergoes regional extension: here the initiation of collapse is coeval to the eruption onset (Gudmundsson 1998, 2007).

5.5 Relationships to Regional Tectonics

Modelling suggests that the structure and development of calderas are largely independent of any regional tectonics. Despite this, regional tectonics may still affect some features, as the caldera shape in map view, generating an elliptical collapse with major axis parallel to the minimum horizontal principal stress σ_m.

These elliptical calderas may develop from elliptical or even circular (in map view) chambers at depth, in any case due to a regional tectonic contribution (Acocella 2007). Most commonly elliptical calderas reflect the shape of anisotropic (elongated) magma chambers at depth. Elongated chambers may form similarly to what observed at borehole breakouts, where the cavity is narrowed along the direction of the maximum horizontal principal stress σ_M and elongated parallel to minimum horizontal principal stress σ_m. This differential horizontal stress may explain the elongation, parallel to the direction of regional extension σ_3, of several elliptical calderas, as along the oceanic ridge of Iceland (Askja, Krafla), the East African Rift System (Suswa, Silali, Paka) and the Taupo Volcanic Zone of New Zealand (Okataina, Taupo; e.g., Bosworth et al. 2003). Elongated magma chambers leading to elliptical calderas may also form through the coalescence of multiple dikes aligned perpendicular to the direction of regional extension σ_3 or intruding pre-existing regional structures. In both cases, the result is an elongated magma chamber growing along the direction of the dikes. Examples of calderas elongated parallel to the rift axis (and thus to the direction of dikes) and perpendicular to the direction of regional extension include Erta Ale and Pantelleria (Italy).

In principle, elliptical calderas may also derive from the collapse of circular (in map view) magma chambers, provided a regional stress field is active. This may occur in three situations (Acocella 2007). (a) When an outward dipping ring fault locally reactivates a pre-existing regional normal fault dipping towards the caldera centre: this shifts the upper part of the ring fault outwards, locally widening the caldera. The reactivation may occur only if the ring fault is tangent to the regional fault. The field relationships between regional normal faults and the western rim of Askja caldera suggest that even a difference in strike of very few tens of degrees hinders reactivation. (b) In presence of an active regional stress field, which affects the dip of the portion of the outward dipping ring fault striking perpendicular to the minimum horizontal principal stress σ_m or to the maximum horizontal principal stress σ_M (Holohan et al. 2005). In particular, the portion of the outward dipping ring fault striking perpendicular to the σ_m direction (extensional condition) becomes steeper, widening the caldera in that direction, whereas the portion of outward dipping ring fault striking perpendicular to the σ_M direction (compressional condition) becomes gentler, narrowing the caldera in that direction. As a result, in both cases a) and b) the major axis of the elliptical ring fault is parallel to the minimum horizontal principal stress σ_m. In any case, the models suggest that with pre-existing regional structures or regional stress field the expected maximum eccentricity is $\sim$1.2. Therefore, only a part of the eccentricity of more elongated calderas may be ascribed to pre-existing regional extensional structures or a regional stress field. (c) A further process possibly generating elliptical calderas from originally circular magma chambers is post-

collapse faulting. Regional normal faults may in fact dissect and elongate a caldera along the minimum principal stress σ_3, as proposed at Fieale, Afar (De Chabalier and Avouac 1994). However, the efficiency of this process appears limited, as highly dipping normal faults do not usually increase caldera eccentricity of more than $\sim 10\%$.

At the extreme, significant magma chamber withdrawal may reactivate regional normal faults, if present, forming graben calderas. **Graben calderas** are elongated rift segments bounded by normal faults collapsing during large eruptions under regional extension and whose width approximates that of the erupting reservoir below. Graben calderas, inferred on continental (southern Basin and Range, western USA), transitional (central Afar) and oceanic rifts (East Pacific Rise), thus represent a strongly elongated end-member type of caldera (Lagabrielle and Cormier 1999; Aguirre Diaz et al. 2008; Acocella 2010). Because of the "space problem", a block bounded only by inward dipping regional faults may not sink: therefore, the reactivation of outward-dipping regional normal faults with inverted (reverse) kinematics is expected.

Finally, regional tectonic stresses may not only affect the caldera shape, but also its anticipated or delayed formation. In fact, numerical results indicate that regional extension decreases the stability of the roof rock overlying a magma chamber, thereby promoting early-onset caldera collapse, or even suppressing any resurgence. Alternatively, moderate amounts of regional compression (≤ 10 mm/year) on relatively short timescales ($<10^4$ years) increase roof rock stability, delaying collapse (Cabaniss et al. 2018).

5.6 Resurgence

Some calderas experience notable uplift of their floor, providing evidence for resurgence. **Resurgence** is a spectacular, albeit still relatively poorly-known, feature of many calderas, so that it is commonly defined on the evident uplift of the caldera floor, rather than on the responsible process(es). The uplift may be recognized from unusually raised deposits within the caldera, including the caldera-forming eruption or marine and lacustrine sediments. The uplifted area is usually circular to elliptical, from a few kilometres (Pantelleria, Italy) to a few tens of kilometres wide (La Pacana, Chile), somehow proportional to the size of the caldera; in some cases, resurgence may show a polygonal shape, due to the reactivation of pre-existing regional structures (Ischia, Italy; Fig. 5.10).

The amount of uplift ranges from a few tens of metres, as at Alcedo (Galapagos), to more than a thousand of metres, as at Valles (New Mexico), Toba (Sumatra) and Cerro Galan (Argentina). The duration and uplift rate of resurgence are usually poorly constrained, being at best inferred through the cumulated uplift achieved within a geologically-defined period (often tens of thousands of years), which is usually longer than that of effective uplift. So far, the best-constrained uplift paths for resurgence derive from Campi Flegrei, Toba, Siwi (Vanuatu) and Iwo-Jima (Japan) (Fig. 5.11; Newhall and Dzurisin 1988, and references therein; Chen et al. 1995; de Silva et al. 2015; Isaia et al. 2019). These cases show very different duration of resurgence, which lasts from ~ 1 to 70 ka, and different uplift rates, which range from centimetres to tens of centimetres per year, that is similar to or one order of magnitude faster than the regional tectonic rates. However, these rates are usually not constant. For example, the resurgence at Campi Flegrei shows uplift episodes alternated with subsidence. While net uplift dominates, the temporary subsidence may be still significant at times, on the order of several tens of metres over a few thousands of years. Also, the eruptive periods (epochs) broadly correlate with periods of uplift during resurgence. At Siwi and Iwo-Jima the available data describe incremental uplift phases interrupted by stases and minor subsidence. The resurgence at Toba shows an apparently continuous, albeit not constant, uplift. Therefore, available evidence indicates that most resurgent uplift occurs episodically, within a very few thousands of years, interrupted by stasis or even subsidence, although some calderas show a more continuous behaviour (Acocella 2019). In some

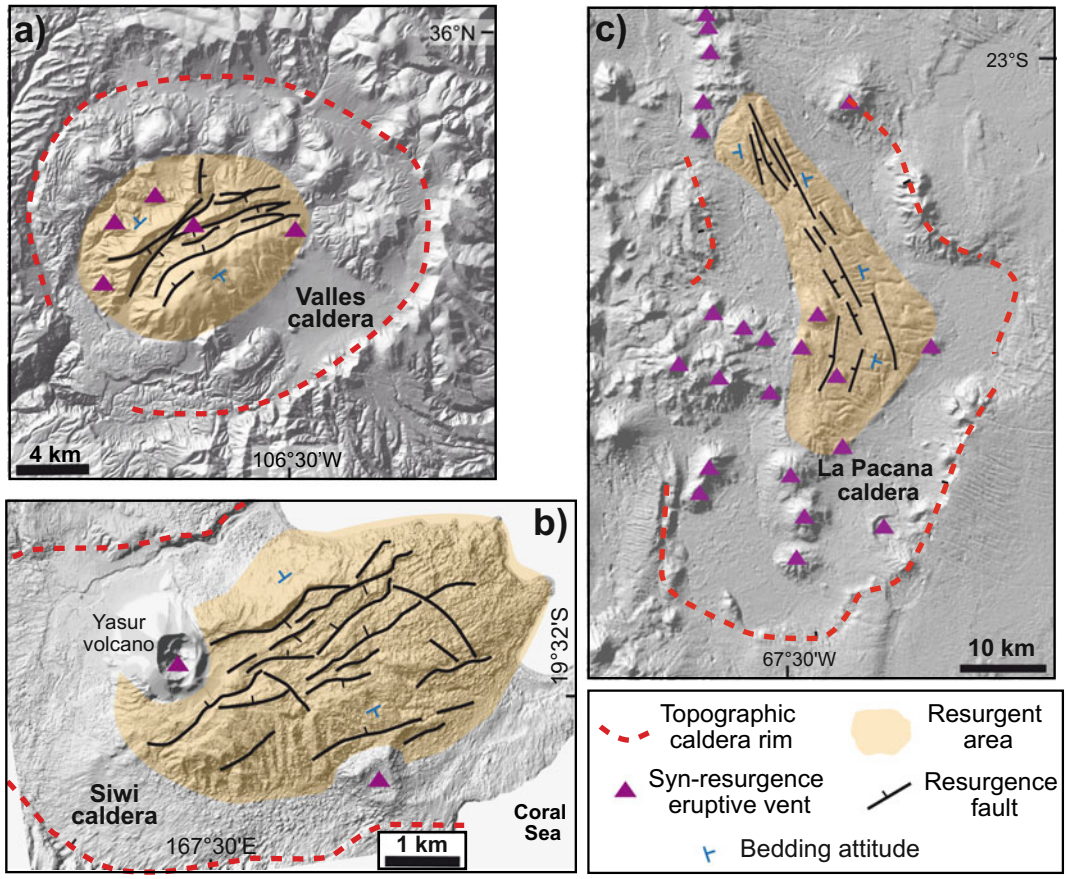

Fig. 5.10 Examples of resurgent calderas; note the different scales. **a** Valles caldera, New Mexico (USA); **b** Siwi caldera, Vanuatu; **c** La Pacana caldera, Chile (Siwi DEM courtesy: Elodie Brothelande; modified after Lindsay et al. 2001; Galetto et al. 2017)

cases, as at Pantelleria and Ischia, geodetic data indicate that the resurgent portion of the caldera has been experiencing subsidence for decades, suggesting an interruption of the longer-term resurgence. At Ischia, the subsidence is accompanied by recurrent, very shallow (~1 km depth) and destructive seismicity along the faults bordering the most uplifted part of the resurgent area. This behaviour may result from accelerations of the ongoing subsidence, which is interpreted to derive from the degassing of the previously intruded and non-erupted magma partly responsible for resurgence (Trasatti et al. 2019). Resurgence is commonly associated with felsic volcanism (Table 5.1). In fact, most of the resurgent calderas, including those with strong uplift reaching a thousand of metres, as at Valles, Long Valley, Toba and Ischia, are consistently felsic. Resurgence in mafic calderas is found only at Loihi (Hawaii) and Alcedo and Sierra Negra (Galapagos), with moderate uplift between ~30 and ~100 m (Acocella 2019; Clague et al. 2019).

In many resurgent calderas the uplifted deposits define a broad subcircular or elliptical **resurgent dome**, associated with an apical graben with inward-dipping normal faults, as observed at Valles, Long Valley or Kutcharo, Japan. The apical graben, often elongated perpendicular to the regional extension direction, results from the crestal extension created by the doming, which may also be responsible for a

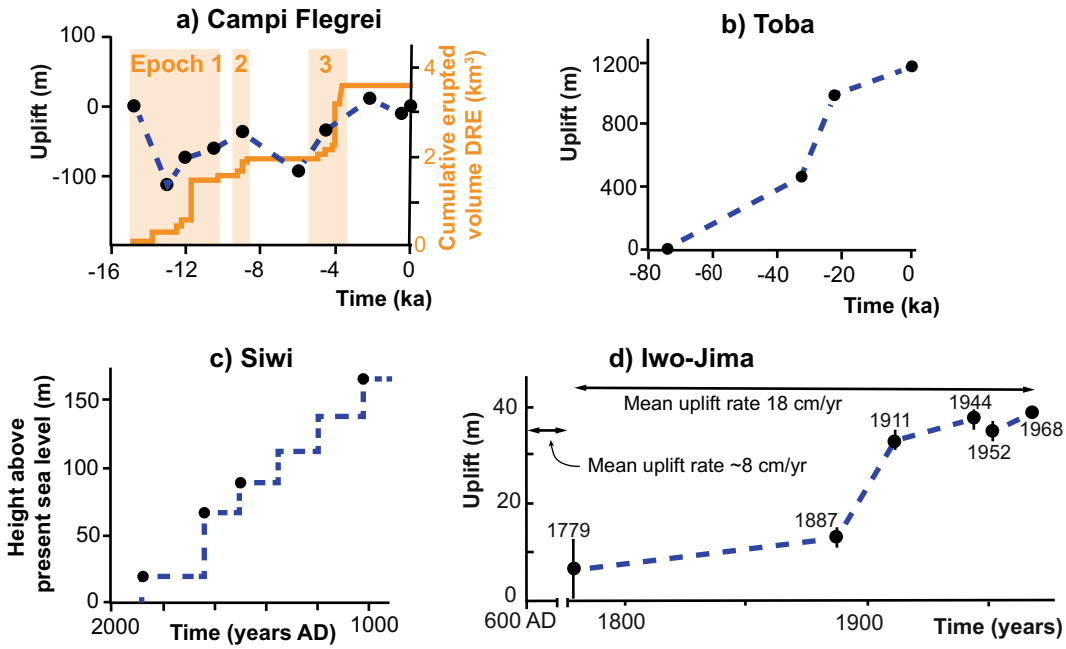

Fig. 5.11 Uplift histories of felsic resurgent calderas at Campi Flegrei (Italy), Toba (Sumatra), Siwi (Vanuatu) and Iwo-Jima (Japan). Eruptive periods (orange bands) and cumulative erupted products (orange curve) are also included for Campi Flegrei (modified after Acocella 2019)

localized decompression promoting the apical volcanism. These domes in fact also show syn-resurgence eruptive vents within the dome and along the boundary, likely resulting from the pervasive intrusion of magma within the dome faults and the resurgence ring fault (Self et al. 1986; Goto and McPhie 2018).

In other calderas the uplifted deposits may define a **resurgent block**, where the non-bended deposits have a consistent attitude. These may be tilted of a very few tens of degrees about a horizontal axis, showing a marked asymmetry in the section view of the block, as at Ischia, Pantelleria, Alcedo, Sierra Negra and Suswa (Orsi et al. 1991; Skilling 1993). Resurgent blocks show syn-resurgence eruptive vents along their sides, in correspondence with the border faults, or outside. The development of a resurgent dome or block does not depend on the amount of uplift, as resurgent blocks may be uplifted as much as domes (Table 5.1). The possibility to develop a resurgent dome or a block may depend on the aspect ratio A_r (thickness z/width L) of the crust overlying the magma chamber (Fig. 5.12; Acocella et al. 2001). Aspect ratios $A_r \sim 1$, where the depth to the magma chamber is similar to the width of the uplifted area, develop resurgent blocks with consistent attitude of the layers and peripheral volcanic activity (Ischia and Pantelleria type). Aspect ratios $A_r \sim 0.4$, where the depth to the magma chamber is smaller than the width of the uplifted area, develop resurgent domes with apical depression, domed layers and peripheral and internal volcanic activity (Valles and Long Valley type). These features may result from the different flexural response of the thicker and thinner uplifted crusts. The large and apparently resurgent block of Toba may provide an exception to this model.

The boundary of the resurgent portion may be sharp and with evident morphological expression, such as a scarp, suggesting the activity of faults confining the uplift. This is well exemplified along the most uplifted part of resurgent blocks, as at Ischia and Pantelleria. Modelling

Table 5.1 Main features of active resurgent calderas

Name	AC (km^2)	AR (km^2)	Uplift (m)	Vr (km^3)	Vv (km^3)	Type	t (ka)	tr (ka)	Composition	Supply	Reg. ext. (mm/year)
Ischia	46	~20	~1000	9 ± 2	<1	B	22 ± 5	<33	T	Yes	< 2
Pantelleria	42	7	~350	1.5 ± 0.3	0.5 ± 0.2	B	27	<18	T, R	Yes	< 2
Campi Flegrei	~200	~30	~250	3 ± 0.5	4 ± 0.5	D	<4	<15	T	Yes	< 2
Long Valley	450	~80	>400	~15	(≪100)	D, G	(100)	(80)	R, Da	Yes	0.6
Valles	283	~65	≥1000	32 ± 5	<5	D, G	(<40)	27 ± 27	R, RD	Yes	< 4
Yellowstone SC	2500	214	?	>27	0	D, G	(<84)	(<123 ± 9)	R	Yes	< 4.3
Yellowstone ML	2500	164	?	20 ± 7	(<600)	D, G	~440		R	Yes	< 4.3
Toba	2350	950	1100	320 ± 30	20 ± 5	B	(<40)	<70	R, Da	Yes	0
Siwi	36	18	>250	4.5 ± 1	0.5 ± 0.3	D, G	(<18)	(2)	Ba, TA	Yes	≥ 0
Iwo-Jima	63	17	>120	>1.5	0	D	(>2)	<0.8	TA	Inferred	< 2

AC Area of caldera; *AR* Area of resurgence; *Vr* Volume of resurgence; *Vv* DRE volume of syn-resurgence volcanism; *B* Block, *D* Dome, *G* Graben; *t* Time between caldera collapse and resurgence; *tr* Duration of resurgence. Composition: *T* Trachyte, *R* Rhyolite, *Da* Dacite, *RD* Rhyodacite, *Ba* Basalt, *TA* Trachyandesite; supply: evidence of new magma supply; reg. ext.: rates of regional extension. Yellowstone SC: Yellowstone Sour Creek dome, Yellowstone ML: Yellowstone Mallard Lake dome. Values in () are poorly constrained and may not be representative

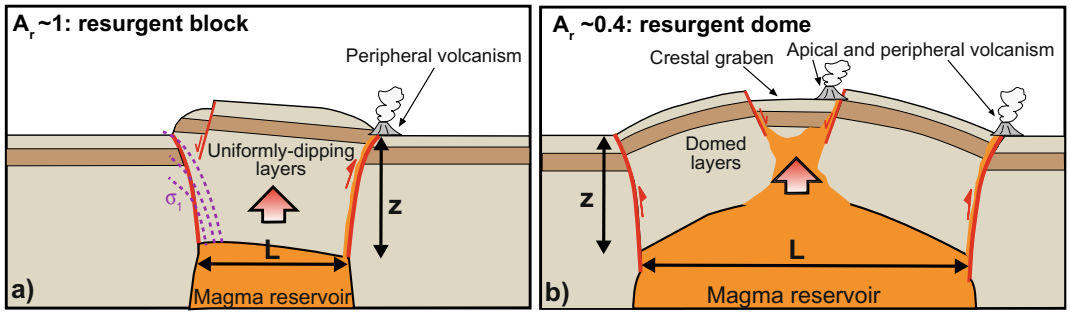

Fig. 5.12 Summary of the two main resurgence modes observed in experiments and nature mainly as a function of the aspect ratio A_r (where A_r = thickness z/width L) of the crust overlying the magma chamber. **a** A higher A_r develops a resurgent block with consistent layers within and peripheral volcanic activity (Ischia and Pantelleria type; dashed purple lines illustrate local configuration of the σ_1 trajectories controlling the development of the reverse ring fault). **b** A lower A_r develops a resurgent dome with domed layers, apical depression and volcanic activity at the periphery and within the dome (Valles and Long Valley type; modified after Acocella et al. 2001)

and field data (as at Valles) suggest that the boundary of resurgent domes may also experience non-elastic deformation, thus being faulted. Therefore, the presence of resurgence bounding faults raises a "space problem" similar to caldera collapse. As a consequence, the nature of the resurgence's bounding faults has been object of field and modelling studies (Tibaldi and Vezzoli 1998; Acocella et al. 2001). Resurgent blocks and domes cannot be bordered by major outward dipping normal faults, as the uplift of a horst-like structure would require unrealistic syn-resurgence extension outside the uplifted area. Therefore, most resurgent areas are expected to be bordered by subvertical to high angle inward dipping, reverse structures. High angle inward dipping reverse faults, with displacement of several hundreds of metres, have been observed to border resurgent blocks, as at Ischia. These features are also common in resurgence experiments, resulting from the upward rotation of the maximum principal stress σ_1 during differential vertical motion, similarly to what occurs for the caldera reverse faults (see detail of stress distribution in Fig. 5.12a). In addition to the reverse faults, marking the structural boundary of the resurgence, internal normal faults may result from the gravitational instability of the periphery of the uplifted area, similarly to what observed for the caldera normal faults.

Resurgence is a notable feature of many calderas. However, while many studies have investigated and explained the causes of caldera collapse, the processes controlling the opposite motion, that is resurgent uplift, have been more rarely investigated and, as such, remain less understood. In fact, while it has been generally accepted for decades that resurgence results from a build up in pressure in the magma chamber, or from shallow intrusions, a few models have been proposed to explain the details of this process. Possible mechanisms related to the dynamics of a magma chamber and triggering resurgence are regional detumescence, magmatic rebound and general magma pressurization (Marsh 1984; Kennedy et al. 2012). **Regional detumescence** is one of the first models proposed for resurgence (Smith and Bailey 1968; Marsh 1984). It implies that, upon caldera formation, an originally inflated crust relaxes, pushing downward on the magma chamber and squeezing magma upward against, around, and possibly through the fallen caldera block, triggering resurgence. This process does not really require any addition of new magma within the chamber and, as such, provides a self-sustaining explanation for resurgence after caldera formation. However, it would require a magma chamber much wider than the collapsed area and relaxation of a large previously uplifted area, features which are not really

observed. Therefore, this model appears unsupported by observations. **Magmatic rebound**, and/or decompression following the formation of a caldera, has been proposed as an attractive and elegant explanation for resurgence (Marsh 1984; Kennedy et al. 2012). This is related to the sluggish response of the viscous magma to the sudden drawdown caused by the eruptions during caldera formation. In particular, the caldera-forming eruption may empty more than enough magma to bring the system to magma-static equilibrium, determining a pressure drop which may be balanced by the flow of new magma injected in the system. In this model, resurgence requires the input of new magma closely following caldera formation. A limitation to the widespread application of this model is that the time between caldera development and the onset of resurgence in natural cases often ranges from a few tens of thousands of years (Ischia, Pantelleria, Valles) to several hundreds of thousands of years (Yellowstone), suggesting the lack of a direct relationship between caldera collapse and resurgence (Table 5.1). **Magma pressurization** is a broad term, which includes an increase in the pressure within a magma chamber as resulting from magmatic convection, vesiculation or the influx of new magma at the base of the caldera block (Smith and Bailey 1968; Marsh 1984). This process usually requires the injection of new magma within the magma chamber, although it may also occur emplacing shallower laccolith-like intrusions, even at the base of the caldera infill. Evidence for such a shallower magma mainly derives from eroded calderas, as at Grizzly Peak and Lake City (Colorado, USA) and Kumano (Japan), and borehole stratigraphy, as at Long Valley (Fridrich et al. 1991; Kawakami et al. 2007; Kennedy et al. 2015; Hildreth et al. 2017). Magma pressure increase within the chamber, or at shallower levels, is a feasible possibility, although alone it still does not explain a crucial feature of resurgence, that is the anomalous accumulation of magma required to trigger dramatic uplift instead of feeding eruptions. This latter feature is underlined by the usually much higher volumes of the resurgent portion with regard to the volumes of magma erupted during resurgence. This imbalance suggests some process hindering the extrusion of the pressurized magma. This problem has been tackled postulating that the hindered eruption of the magma responsible for resurgence is related to its relatively low viscosity contrast (less than approximately 9 orders of magnitude) with the residual magma below a caldera (Galetto et al. 2017). Such a viscosity contrast provides a rheological barrier, hindering the upward propagation through dikes of the new injected magma, which accumulates in sill- or laccolith-like intrusions, stagnates and promotes resurgence (Fig. 5.13). This model considers a spectrum of combinations in the thickness and viscosity of the residual magma, which determine the permeability of the rheological barrier. Thicker and medium viscosity residual magma provides a less permeable barrier, leading to resurgence without eruptions within the resurgence area, as observed at Ischia, Yellowstone or Iwo-Jima. Other conditions of thickness and viscosity provide a more permeable barrier, leading to resurgence accompanied by diking and thus eruptions within the resurgent area, as observed at Campi Flegrei. This mechanism may explain resurgence through the input of new magma at different crustal levels, as within the magma chamber or at the base of the caldera infill. A neutral or compressive regional stress field would further hinder dike propagation and eruptions, thus encouraging the storage of the magma at depth and resurgence, consistently with the evidence that resurgent calderas are rare or absent in rifts experiencing relevant extension (several mm/yr or more, as in the Taupo Volcanic Zone of New Zealand). Similar low-viscosity contrasts in magma reservoirs may also provide the conditions to pass from magma eruption to accumulation, which is essential to develop large magma chambers before major eruptions.

5.7 Caldera Unrest

A distinctive shorter-term behaviour of calderas is their frequent state of unrest, as revealed by surface deformation, seismicity and degassing.

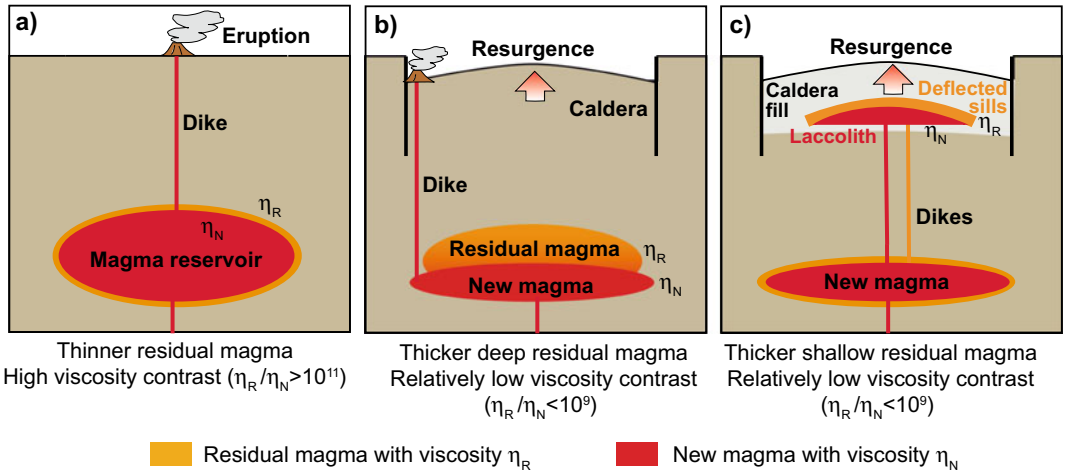

Fig. 5.13 Conditions for resurgence. **a** A thinner layer of viscous residual magma (high viscosity contrasts with the new magma) promotes dike propagation and eruption, without resurgence**. b** A thicker layer of medium viscosity residual magma (with relatively low viscosity contrast with the new magma) hinders dike propagation, promoting stagnation and resurgence; peripheral eruptions may occur. **c** Same as (**b**), but shifted at shallower levels: dikes (orange) may arrest within the altered intracaldera tuff, developing one or more sills (orange) constituting a rheological barrier for successive dikes (red), stagnating in laccoliths and promoting resurgence. Mechanism (**c**) may be alternative to, or combined with, (**b**) (modified after Galetto et al. 2017)

Unrest is a deviation, lasting from days to centuries, from the normal quiescent state towards a state which may lead to eruption. Unrest, although most common at calderas, may occur at any volcano, representing a widespread condition. Because of its general occurrence and potentially hazardous implications, unrest is discussed, together with eruption forecasting, in Chap. 9; here only an overview of the specific caldera unrest features is given.

More than a thousand episodes of caldera unrest have been documented based on the appearance of phenomena related to the eruption preparation, or possible precursors. As in a typical year some form of unrest occurs at nearly 20 calderas on average, unrest should be considered a common state for active calderas, although in approximately half of the cases unrest does not culminate into eruption (Phillipson et al. 2013). The most frequently reported features characterizing caldera unrest include local earthquake swarms, volcanic tremor; uplift, subsidence, tilt, ground fissuring, changes in the temperature of soil, water, or gas, changes in fumarolic activity and, ultimately, eruptions. These seismic, geodetic, geochemical and thermal variations are mostly limited to parts of calderas, without being necessarily concentric. But seismicity, uplift, degassing, thermal activity and eruptions at a given caldera do not always share a common centre. Furthermore, centres of each unrest may shift from one episode to the next, or even within a single episode. At depth, unrest may reach the lowermost crust (Newhall and Dzurisin 1988; Acocella et al. 2015; Hotovec-Ellis et al. 2018).

In particular, as regards surface deformation, all types and scales of ground deformation may occur in any part of a caldera during unrest. Occasionally, ground deformation above a conduit or a dike is so dramatic that it can be directly witnessed without any instrument. Normally, however, ground deformation is subtle and within the elastic domain (with rates of millimetres or centimetres per year), so that it can be detected only through appropriate equipment (see Chap. 8). Broad, subtle, years to decades long uplift has occurred within several large calderas. A common deformation pattern consists of a dome-like inflation, with the maximum uplift centred on an internal portion of the caldera.

Surface deformation can be usually modelled with sources shallower than 10 km depth, consistent with the depth to the top of large geophysically imaged magmatic reservoirs (Newhall and Dzurisin 1988).

As regards seismicity, this may be found around caldera margins and elsewhere within the caldera. Most seismic swarms within or near calderas consist of relatively small earthquakes, with magnitude lower than 3 and rarely reaching 6 and depth less than 15 km. Some of these result from the brittle failure of country rock under magma intrusion (volcano-tectonic earthquakes, see Sect. 8.4.1). Failure may be facilitated by high pore pressures within hydrothermal systems. Other events reflect release of regional tectonic stress, shear of viscous magma along the walls of a conduit, explosions in magma, or collapse as magma is erupted or drains laterally into a rift zone, producing low period events and volcanic tremor (see Sect. 8.4.1). Eruptions can occur at any stage in the waxing or waning of seismic energy release: patterns are too varied and too poorly understood to conclude that any specific behaviour will lead to eruption. Also, the intensity of precursory seismic activity is not always proportional to the size of any associated eruption (Newhall and Dzurisin 1988).

As regards degassing, this may occur in any part of the caldera, also outside. Within this variability, degassing usually focuses in defined portions of the caldera, as vents, craters or along fault zones, largely depending upon increased local permeability conditions. Changes are commonly noted in fluid composition, flux of fumaroles or hot springs, level and composition of ground water, or water level in crater lakes. The most common changes are increases in total discharge, in the discharge and proportion of acid gases (SO_2, H_2S, HCl and HF) and in CO_2 emission. Also, several calderas have major thermal areas on their floors or along their rims, as Yellowstone and Uzon (Kamchatka, Russia). Temperatures of fumaroles range from less than 100 °C to more than 950 °C, and temperature changes of several hundred degrees are not uncommon during unrest. Temperature changes have been reported for several caldera lakes (Newhall and Dzurisin 1988).

Caldera unrest usually persists for months to years, and sometimes even decades to centuries. Unrest is usually longer at silicic calderas, possibly resulting from the higher viscosity and larger size of silicic magma systems, which slow any response to disturbance. Some unrest at large calderas, such as Campi Flegrei, Rabaul (Papua New Guinea), Aira and Iwo-Jima (Japan), has been lasting for centuries (Newhall and Dzurisin 1988; Jellinek and DePaolo 2003; Dvorak and Dzurisin 1997). Unrest is likely to be intermittent, rather than to show a systematic increase until culmination. In fact, during unrest activity may wax or wane several times before culminating in any eruption or a shallow intrusion or before returning to quiescence (Fig. 5.14). Seismicity often occurs in repeated swarms, rather than in a continuous pattern and uplift often alternates with subsidence (as at Yellowstone and Campi Flegrei) and may be episodic, as suggested by the multiple terraces at Toba and Iwo-Jima. The intermittent nature of most unrest at calderas poses a challenge for eruption forecasting, because successful forecasts must distinguish between short lulls and long periods of quiescence in order to be socially useful.

Caldera unrest reflects tectonic, magmatic and hydrologic processes. However, where established, the root cause for unrest is magmatic. While external earthquakes or hydrothermal processes may definitely encourage unrest, no unrest is of purely hydrothermal or tectonic origin: magma appears as the main ingredient, although in many cases it may also induce important changes in the hydrothermal system, supplying this with fluids and energy (Newhall and Dzurisin 1988; Acocella et al. 2015). As a result, it may become difficult to define whether unrest has a dominant magmatic or hydrothermal involvement, although the outcome of one condition or the other may be different. If the hydrothermal component dominates, a phreatic eruption may be the expected outcome from the pressurization of the hydrothermal system. Conversely, the involvement of a dominant magmatic component may lead to a stronger and more

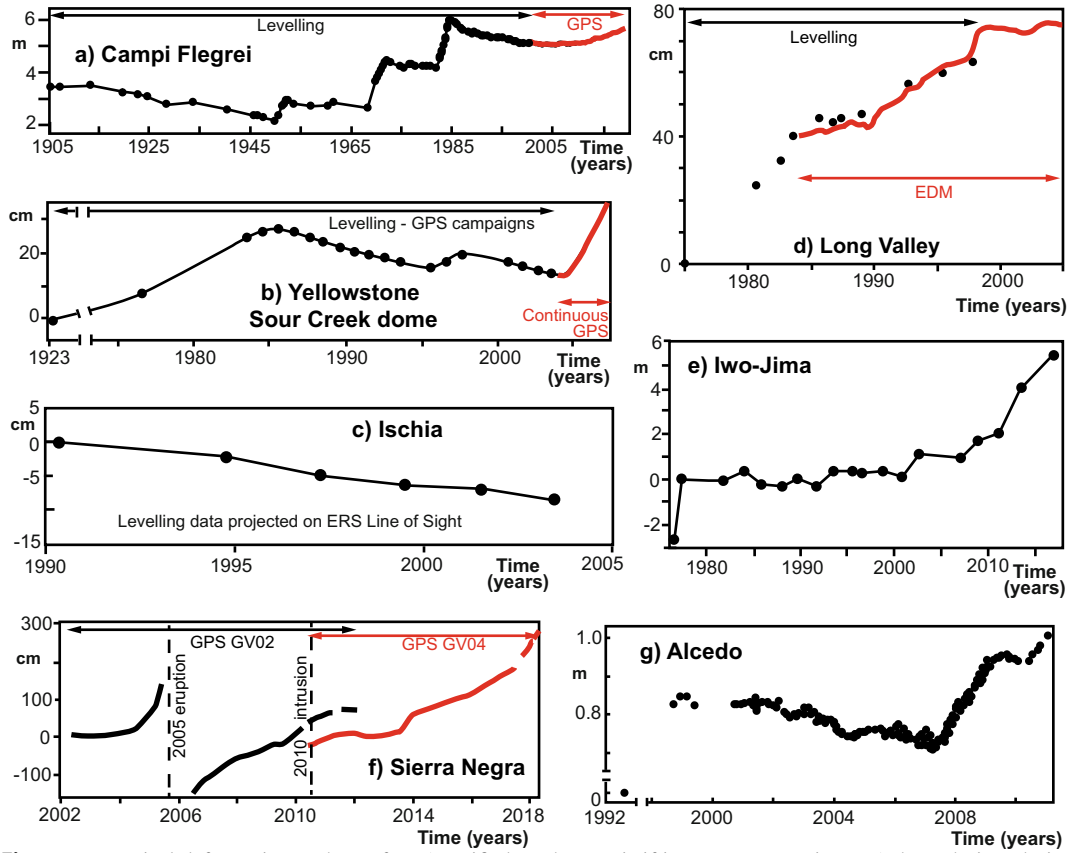

Fig. 5.14 Vertical deformation at the surface (specified on the *Y*-axis if in metres or centimetres) through time during unrest episodes at felsic (**a**–**e**) and mafic (**f**, **g**) resurgent calderas (modified after Acocella 2019)

impacting magmatic eruption. Therefore, while discriminating the nature of the dominant unrest component is challenging, it is also important for appropriate hazard assessment and eruption forecasting. The recommendation is to combine multiple types of observations, as no one type of data uniquely pinpoints the nature of unrest (Pritchard et al. 2019). Among the various approaches, the inversion of volcano deformation data contributes to distinguish pressurized magmatic from hydrothermal sources, constraining their location, volume change and shape (see Sect. 8.3.2). In fact, a first-order distinction between a dominant magmatic or hydrothermal involvement in unrest should consider the depth of the retrieved source: if this is larger than 3–4 km, then chances are that the hydrothermal system has minor involvement. Magmatic unrest at calderas is often consistent with pressurised sill-like intrusions or oblate (with minor vertical axis) ellipsoids (see Chap. 9). In the case of repeated and intermittent unrest, recurrent magma emplacement should be considered. This condition requires a persistently hot crust, where magma emplacement is assisted by the thermal anomaly created by the previously intruded magma (Amoruso et al. 2017). Sometimes more than one dominant source is needed to explain observations, highlighting complex distributions of melt in the shallow plumbing system, especially below silicic calderas. Caution should be also taken in interpreting the caldera deformation data for geodetic inversion. In fact, some calderas have shown patterns of surface deformation consisting of broad subsidence affecting the wider volcanic edifice and stronger localized subsidence focused inside the caldera ring faults. Physical models in elastic half-space (see Sect. 8.3.2) commonly explain these observations with the

pressurization of two magma sources at different depths. However, taking into account for the deformation along the ring fault, both the broader and the more focused subsidence can be explained by the shrinking of a same deeper magma source, above which the activity of the ring-fault localizes the deformation at the surface. Therefore, omitting ring faulting and using multiple point/sill-like sources in models of subsiding (or inflating) calderas can result in erroneous estimates of magma reservoir depths and volume changes (De Natale and Pingue 1993; Liu et al. 2019).

5.8 Long- Versus Short-Term Deformation

Many calderas show the superimposition of longer-term geological uplift (hundreds to thousands of years; during resurgence) and shorter-term geodetic deformation often characterized by uplift (years to decades; during unrest), frequently insisting on the same area (Fig. 5.15). These uplifts refer to different timescales and can be detected only through different approaches: therefore, trying to understand the relationships between the longer- to the shorter-term uplift, as well as the responsible processes, is not straightforward. In fact, resurgence has been often assumed to result from a continuous, although not necessarily constant, uplift, related to a single or anyway distinct supply of magma. Conversely, unrest is accompanied with a more discontinuous behaviour, characterized by statis and deflation episodes. This apparently different behaviour has suggested that resurgence is a distinct process, independent of unrest in mechanism and scale (e.g., Marsh 1984; Kennedy et al. 2012; de Silva et al. 2015).

Comparing the shorter- and longer-term deformation histories at resurgent calderas provides an alternative understanding of these

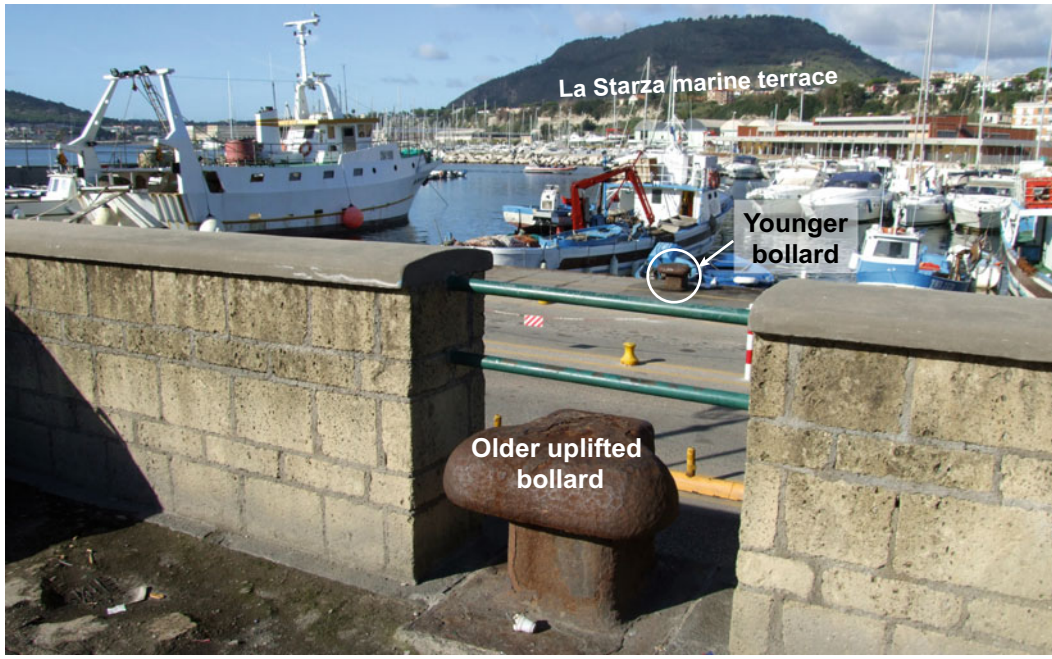

Fig. 5.15 Example of notable shorter- and longer-term deformation at Campi Flegrei caldera, Italy. Foreground: older dock level of the Pozzuoli harbour, in the caldera centre, uplifted of ~2 m during the 1982–1984 unrest, with the newer and currently active dock level, built after the unrest, lying approximately 2 m below; both docks are identified by the bollards. Background: La Starza marine terrace, uplifted of at least 60 m during resurgence of the caldera centre (photo courtesy Mauro Di Vito)

relationships. Available data show that, on the short-term, unrest at resurgent calderas (Long Valley, Yellowstone, Ischia, Campi Flegrei, Iwo-Jima, Sierra Negra, Alcedo) consists of uplift and subsidence, with the former dominating and producing net uplift (Fig. 5.14). On the long-term, the uplift history of the known resurgent cases (Campi Flegrei, Iwo-Jima, Toba and Siwi) includes, in addition to prevalent uplift, also stasis and subsidence episodes (Fig. 5.11). Therefore, both the short- and long-term deformation histories at resurgent calderas reveal distinct and repeated uplift episodes, highlighting an incremental behaviour. Also, in most resurgent calderas (Long Valley, Campi Flegrei, Iwo-Jima, Sierra Negra and Alcedo) the short- and long-term uplifts coincide in location and pattern. All these similarities suggest that unrest is an incremental episode of the much longer and cumulative resurgence (Acocella 2019). This would imply that resurgence is not the result of a constant, and not even continuous, uplift independent of unrest. Rather, the vertical deformation during resurgence may be interpreted as a combination of episodes of uplift, repose and subsidence, each with different duration, in which net uplift predominates on the longer-term. Also, consistently with the likelihood that caldera inflation results from magma emplacement, each uplift episode during resurgence may be interpreted as resulting from a pulse of magma intrusion. This view supports an incremental growth of magmatic reservoirs, where each episode of inflation may result from the emplacement of a sill-like intrusion, eventually developing a laccolith responsible for resurgence. This frame is consistent with observations from the growth of plutonic bodies, confirming that volcanic and plutonic processes are characterized by similar incremental growth modalities (see Chap. 4; Glazner et al. 2004; De Saint Blanquat et al. 2011; Coleman et al. 2016).

Therefore, resurgence seems the result of a complex longer-term evolution of a magmatic reservoir, in which repeated episodes of shallow magma emplacement responsible for net uplift predominate over possible episodes of stasis or subsidence. In this frame, during resurgence magma intrusion may be followed by quiescence (suggested by a stasis in the deformation), lateral magma propagation (suggested by short-lasting subsidence in the caldera centre), degassing and crystallization (both suggested by long-lasting subsidence), eruption (suggested by abrupt subsidence) or by a new episode of intrusion (suggested by a different uplift rate; Fig. 5.16).

This vision may also contribute in determining the capacity of volcanoes to store or erupt magma, forecasting their longer-term eruptive behaviour. In particular, the coupling or not between uplift episodes and eruptive periods during resurgence at calderas should allow understanding whether or not and, mostly, to which extent, a caldera is able to store its shallow magma. For example, Campi Flegrei highlights a coupling between uplift and eruptions during resurgence (Fig. 5.11a). This is in line with the minor resurgence with $\sim$180 m of uplift and the relatively high amount of magma erupted during resurgence (compare the erupted and resurgent volumes in Table 5.1), suggesting that a relevant part of the magma intruded during resurgence is erupted. However, most resurgent calderas are characterized by a proportionally lower amount of magma erupted during resurgence, whose uplift episodes are expected to be less coupled, or even uncoupled, to eruptions. These diverse behaviours may be related to the different permeability of the residual magmatic reservoir to the new injected magma, as discussed in Sect. 5.6.

5.9 Magma Transfer and Eruptions

After having considered the long-term (resurgence) and short-term (unrest) accumulation of magma below calderas, this section discusses how the accumulated magma may be transferred, eventually feeding eruptions. More detailed aspects of shallow magma transfer below calderas, dealing with circumferential intrusions, are discussed in Sect. 7.5.

Calderas are associated with the largest eruptions. Indeed, they are capable of erupting the hundreds or thousands of km^3 of magma typical of a super-eruption, which is the most destructive

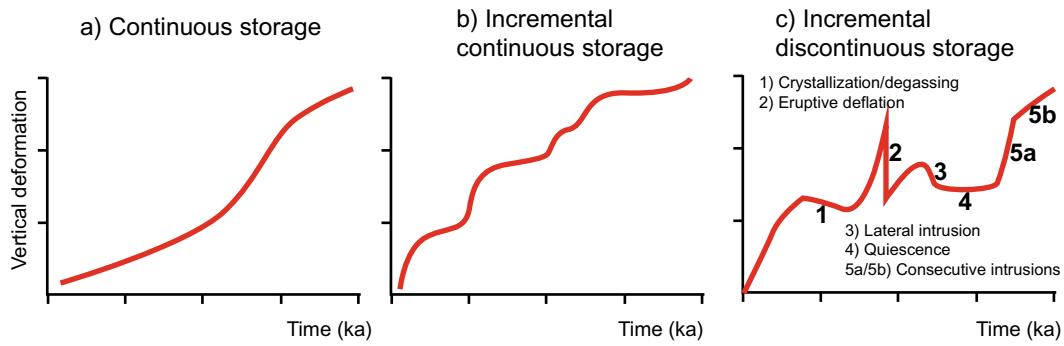

Fig. 5.16 Possible deformation models for resurgence. The incremental discontinuous storage model (case c) is more consistent with available deformation data: here net uplift is interrupted by possible stasis (quiescence) or subsidence, due to crystallization/degassing, eruptions or lateral intrusions, all included within resurgence (modified after Acocella 2019)

natural disaster associated with the activity of our planet. These cataclysmic events are relatively rare, occurring on average less than once every several tens of thousands of years. More frequent (occurring once every approximately 110 years) are the moderate-sized caldera-forming eruptions, as in 1991 at Pinatubo (Philippines; Newhall et al. 2018; Rougier et al. 2018). These moderate to large explosive eruptions are related to calderas because a significant ($\geq 10^1$ km^3 in volume) and rapid (days to weeks) removal of magma from a chamber often generates roof collapse.

The structural features of a caldera may not affect the size of an eruption, but may influence the transfer of magma feeding the eruption. These features are mainly related to the variations in the aspect ratio of the roof of the magma chamber A_r (where A_r is the ratio between the depth z and width L of the crust overlying the chamber; see for example Fig. 5.12) and the amount of subsidence s with regard to the caldera diameter d, expressed as the s/d ratio. While the roof aspect ratio A_r mainly regards larger caldera-forming eruptions, the subsidence/diameter ratio s/d is mainly applicable to minor eruptions, not necessarily related to caldera formation.

As far as the aspect ratio A_r of the roof of the magma chamber is concerned, when $A_r < 1$ the volume of the depression created at the surface is similar to that lost within the chamber during collapse. This implies a $\sim$ 1:1 ratio between the caldera depression volume and the chamber contraction. Conversely, when $A_r > 1$, the volume of the caldera at the surface becomes smaller than the volume lost in the chamber, because of the incoherent deformation developed in the thicker roof. In this case, the ratio between the caldera depression and the chamber volumes becomes less than 1, in line with the previously mentioned (Sect. 5.3) evidence that a larger volume of magma must be extruded at greater depth to form a caldera. For very high aspect ratios, a caldera may not even form at the surface (Fig. 5.17; Roche and Druitt 2001; Geyer et al. 2006). It follows that deeper and narrower magma chambers must evacuate a larger percentage of magma to reach a caldera structure similar to that of shallower and wider chambers.

Another factor related to the aspect ratio A_r regards the effective connectivity between the magma chamber and the surface during a caldera-forming eruption, potentially controlling syn-collapse eruptive activity (Acocella 2007). Lower aspect ratios ($A_r < 1.6$) form coherent collapse, ensuring connection from the chamber to the surface with newly formed gaping faults, which may be penetrated by the magma creating a continuous ring conduit and feeding vents capable of sustaining the eruption. Higher aspect ratios ($A_r > 1.6$) form incoherent collapse, which may hinder appropriate magma penetration, and thus connection from the chamber to the surface and, eventually, the continuation of the eruption, if the eruption is not of relevant size. Therefore,

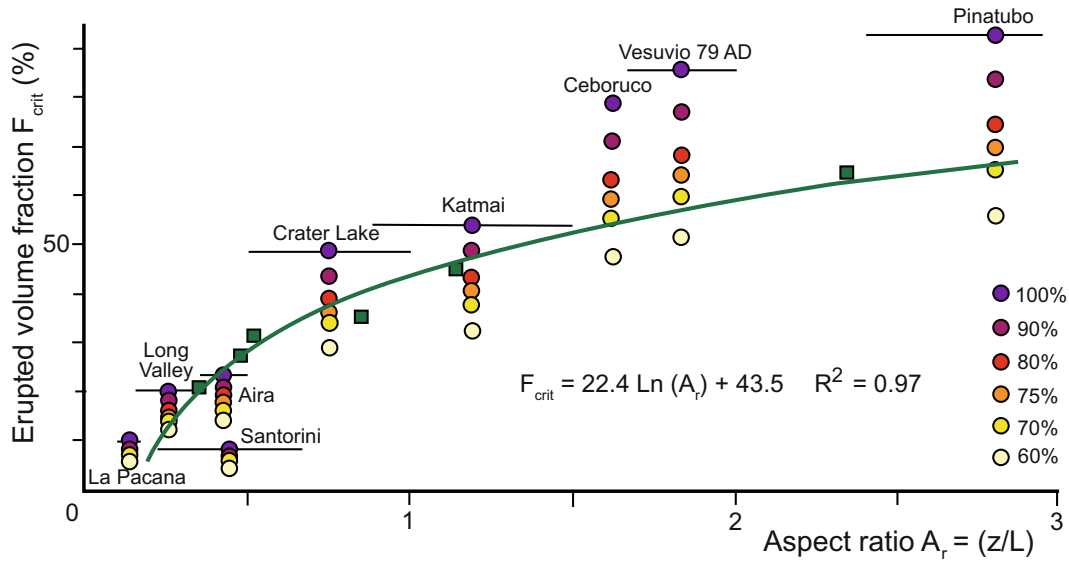

Fig. 5.17 Erupted volume fraction (F_{crit}) at the caldera onset as a function of the aspect ratio of the roof of the magma chamber A_r (where A_r = thickness z/width L of the roof). The erupted volume fraction is the portion of magma that needs to be erupted to trigger caldera collapse. Values of F_{crit} for natural examples are calculated considering different percentages (60–100%) of erupted magma; green squares indicate experimental values of F_{crit} at the collapse onset and green line indicates the related log-fit (modified after Geyer et al. 2006)

in addition to the availability of eruptible magma, the aspect ratio of the chamber roof should be considered as a factor capable of sustaining smaller eruptions.

The occurrence and location of syn- to post-collapse volcanism may also depend on the aspect ratio of the roof of the magma chamber coupled with the *s/d* ratio. A small *s/d* ratio ($s/d < 0.05$) generates downsag without ring fault. In this case, magma withdrawal is expected along the vent responsible for the eruption and/or pre-existing structures. With larger *s/d* ratio ($s/d > 0.05$), the roof aspect ratio A_r becomes important to control the eruption. In the case of shallow and wide magma chambers ($A_r < 1$), the ring faults easily reach the surface and the caldera structure may provide an effective path for the withdrawal for the magma. In this case, if the chamber is experiencing underpressure, the outward dipping ring faults may be preferably intruded during immediate post-collapse activity. This process may have occurred during the 700 km^3 Bishop Tuff super-eruption, at Long Valley. Here the strong ellipticity of the caldera may have favoured the reconstructed pattern of vent migration and ring fracture unzipping, with the maximum failure shear strain along the shorter axis of the elliptical caldera (Holohan et al. 2008). The intrusion of magma along the deeper part of the ring faults may depressurise the nearby portion of the chamber, enhancing the sinking of its roof and triggering a feedback between intrusion and collapse. Any intrusion along inward dipping ring faults requires a higher pressure, as a larger part of the caldera roof has to be uplifted against gravity. This may explain the common occurrence of post-caldera vents along the outward dipping ring fault of mature calderas. Conversely, in the case of larger roof aspect ratio A_r ($A_r > 1$), and still with large *s/d* ratio ($s/d > 0.05$), the condition for the establishment of an effective path for magma withdrawal may not be met. This occurrence depends, for a magma chamber with width L, on the amount of subsidence s with regard to the depth of the magma chamber z, so that a deeper chamber requires a larger subsidence to ensure connection with the surface, as previously explained.

As far as the *s/d* ratio is concerned, this also allows defining the distribution and intensity of the gravitational stresses beneath the caldera. These result from the mass excavation due to the caldera depression, which effectively unloads the crust and reorients the principal stresses, with a subvertical minimum principal stress σ_3 below the caldera centre gradually rotating and becoming subhorizontal below the caldera rim (Corbi et al. 2015; Gaete et al. 2019; Rivalta et al. 2019). The larger the subsidence *s*, the stronger the **unloading** (removal of mass due to the caldera depression), and the larger the caldera width *d*, the deeper the effect of such stress reorientation. However, subsidence depth should be corrected for the presence of any caldera infill (including any water from lakes, sea or ice), accounting for its density difference with the surrounding basement. Therefore, while in general a large subsidence *s* promotes a stronger stress reorientation, this behaviour may be less pronounced in filled calderas, depending upon the thickness and density of the infill. As magma propagates through magma-filled fractures oriented perpendicular to the least principal stress σ_3, this unloading affects the direction of magma propagation, so that any magma-filled fracture ascending below the caldera centre, as a dike, may be deflected towards the caldera rim: the higher the unloading, the stronger the deflection (Fig. 5.18; Gaete et al. 2019). This process is further described below considering two-end members, as Fernandina, a mafic caldera with evident topographic expression at the top of a volcanic edifice, and Campi Flegrei, a felsic caldera largely filled by post-collapse eruptive deposits, without evident edifice.

Fernandina hosts a $\sim$1 km deep and 6.5 $\times$ 4 km wide caldera, as well as circumferential eruptive fissures just outside the caldera rim and radial fissures on the outer slopes of the edifice (Simkin and Howard 1970; Chadwick and Howard 1991). The possible processes controlling this distinctive fissure pattern have been explored considering principal stress orientations. Studies have addressed the effect of magma chamber pressurization, the superposition of regional and magma chamber stresses, or the stress reorientation caused by gravitational loads of the volcanic edifice. An important contribution derives from the evidence that stresses due to the gravitational loading of a volcanic edifice are generally larger than magma chamber pressurisation stresses. For realistic edifice and magma chamber pressurisation levels, edifice stresses dominate everywhere except very close to the magma chamber walls (Roman and Jaupart 2014). In addition, recent geodetic data at Fernandina suggest the circumferential fissures have been fed by laterally propagating sills beneath the caldera, which progressively increased their dip becoming sheets and, subsequently, dikes (see Sect. 7.5; Bagnardi et al. 2013). These features underline the importance of the caldera depression of Fernandina in generating unloading with subvertical σ_3 at depth, promoting sill emplacement and lateral magma propagation. In particular, the rotation towards a subhorizontal σ_3 approaching the caldera rim (where the unloading effect vanishes) affects the lateral propagation of magma, passing from sills to inclined sheets and finally to subvertical circumferential dikes (Fig. 5.19; Corbi et al. 2015).

If the nucleating sill is slightly deeper, it rotates about its propagation direction to adjust to the circumferential σ_3 along the outer slope of the volcanic edifice, so that the resulting feeder dike becomes radial and vertical. Therefore, at Fernandina the superposition of an unloading stress within the caldera (responsible for a vertical σ_3 in the centre and a radial σ_3 at the rim) with a gravitational stress along the outer slope of the edifice (responsible for a circumferential σ_3; see Sect. 7.6.1) controls the distinctive pattern of circumferential fissures outside the caldera rim and radial fissures on the volcano flanks, respectively. A similar behaviour is observed at the other active Galapagos calderas, which share similar topographic features to Fernandina.

Campi Flegrei caldera, on the other hand, has a very different topographic signature. It is a $\sim$12 km wide depression hosting two nested calderas formed during eruptions at $\sim$39 and $\sim$15 ka. The subsidence associated with both depressions is on the order of $\sim$2 km. However, the sea, marine deposits and post-

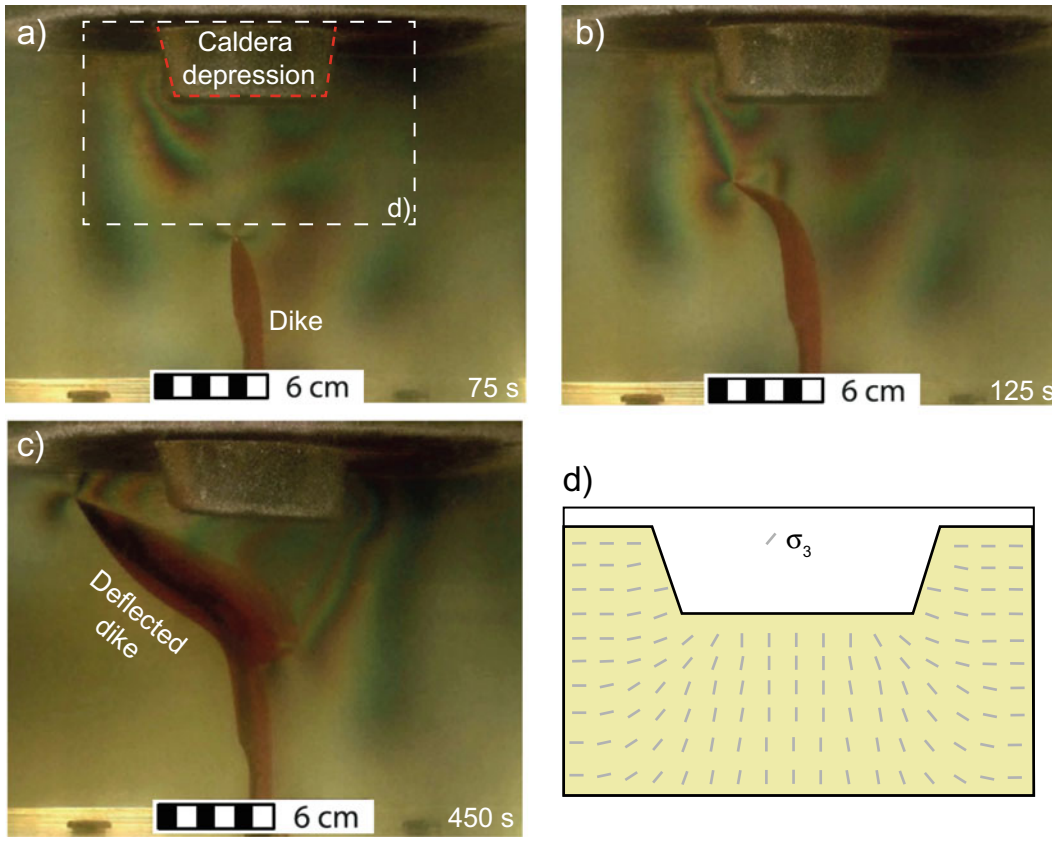

Fig. 5.18 **a**–**c** Section views in polarized light of three stages (running time indicated in seconds at bottom right) of an experiment where red water (simulating magma) is injected in gelatine (simulating the upper crust), highlighting the progressive deflection of the resulting dike below the depression imposed at the surface (red dashed line; simulating a caldera). **d** Simplified sketch of the trajectories of the minimum principal stress σ_3 acting below the depression, illustrating the induced unloading responsible for the deflection of the dike, which orients perpendicular to σ_3 (modified after Gaete et al. 2019)

collapse volcanism filled the caldera depression. In particular, post-caldera volcanism developed more than 70 monogenic vents focused predominantly in the northeast, presently onshore, sector of the caldera. Eruptive activity migrated progressively inward over Epochs 1 (15–9.5 ka), 2 (8.6–8.2 ka), and 3 (4.8–3.7 ka), filling most of the caldera (Orsi et al. 1996; Di Vito et al. 1999; Smith et al. 2011). The vent of the last Monte Nuovo eruption (occurred in 1538) lies just outside the central part of the caldera, but within its rim. Immediately before the last eruption, the intruded magma migrated laterally from an oblate chamber below the caldera centre to beneath Monte Nuovo and then propagated upward feeding a circumferential dike (Fig. 5.20; Di Vito et al. 2016). This limited lateral magma transfer, feeding an intra-caldera eruption, results from the minor difference in topography of the filled caldera, of a very few hundred of meters, and the slightly lower density of the caldera infill, which impose a relatively weak unloading. A limited lateral propagation is observed also for the vents of the last eruptive epoch, which cluster at a similar distance of ~3 km from the caldera centre (Di Vito et al. 2016).

Therefore, Fernandina and Campi Flegrei show how calderas with different topographic expression (deriving from different amounts of subsidence and caldera infill) determine different

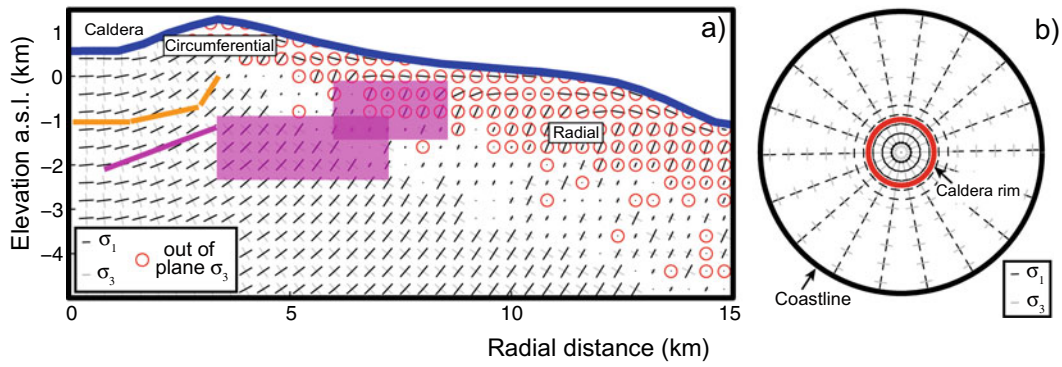

Fig. 5.19 Results of finite element models for an isotropic edifice subject to unloading applied to Fernandina caldera and edifice (Galapagos). **a** Axisymmetric plane projection; the orange lines and the purple line and rectangles represent the projections on the axisymmetric plane of the magmatic sheets feeding the 2005 and 2009 eruptions; note that the purple rectangles represent projections of shallow dipping sheets. The stress components controlling the propagation of the intrusions and resulting from caldera unloading and the load of the volcanic edifice are specified in the inset. **b** Map view distribution of the stress trajectories within the volcanic edifice calculated at sea level (modified after Corbi et al. 2015)

unloading, stronger at Fernandina and weaker at Campi Flegrei. A stronger unloading may drive the magma farther from the caldera centre (outside the caldera rim, Fernandina), whereas a weaker unloading drives magma nearer (intracaldera, Campi Flegrei). The distal or proximal transfer of magma and, ultimately, the location of eruptive vents at calderas depends, in addition to the unloading stresses, also on the regional stresses, the depth to the magma chamber and magma buoyancy. While regional compression (horizontal σ_1) is expected to promote gentler dike trajectories leading to eruptions outside the caldera rim, regional extension (horizontal σ_3)

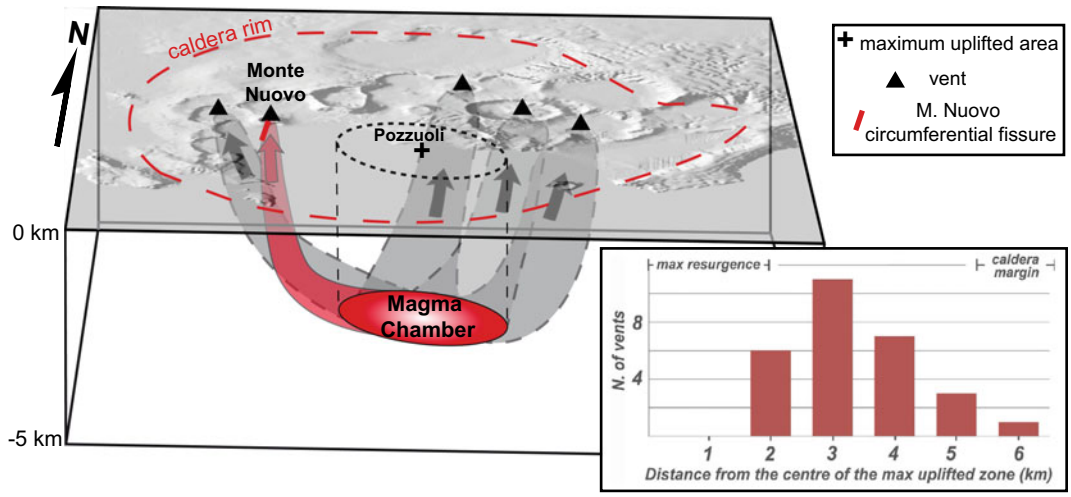

Fig. 5.20 Magma transfer below Campi Flegrei caldera (Italy) before the 1538 AD Monte Nuovo eruption: magma first propagated laterally from the oblate magma chamber at ~4.7 km depth below the caldera centre and then propagated vertically (red path) to feed the Monte Nuovo eruption. The inferred paths (in grey) for other representative eruptions of the last 5 ka are also reported. Inset at bottom right shows the distance from the caldera centre of the eruptive vents active in the last 5 ka: all vents cluster slightly outside the caldera centre, due to the moderate caldera unloading (modified after Di Vito et al. 2016)

has the opposite effect, steepening dike trajectories and promoting proximal eruptions. Also, a deeper magma chamber implies a longer feeder dike and, in turn, a higher magmatic pressure, which inhibits the lateral propagation of sills and promotes dike propagation. A similar effect is played by the buoyancy of the intruded magma, with more buoyant magma inhibiting the lateral propagation of sills and weakly buoyant magma feeding inclined sheets (see Sect. 7.5; Corbi et al. 2015; Gaete et al. 2019).

This rationale may be used to forecast the location of future eruptive vent at calderas. The trajectories of magma propagation are in fact controlled by the stress field within the caldera, which results from the following components: stresses due to the evolution of the volcano (including unloading), tectonic or regional stress, flank movements, magma chamber pressurization, previous intrusions and previous large earthquakes (see Sect. 7.2). The relative importance of these contributions may vary significantly, and determining their weight may be challenging. However, these contributions may be constrained comparing modelled magma trajectories with the location of the eruptive vents. The outcome is a probabilistic stress field which can be used to define magma propagation trajectories and thus probabilistic eruptive vent maps. This procedure has been applied to the post-caldera vents at Campi Flegrei (Rivalta et al. 2019). Here, after the last caldera collapse at ~15 ka, the eruptive vents progressively migrated from the caldera rim inwards. This feature is explained as due to the decrease in the unloading stresses within the caldera, due to its progressive filling in the last 15 ka (Fig. 5.21). Progressive caldera filling has thus weakened unloading stresses and made them less dominant, steepening the dike trajectories and determining the inward migration of the vents in the three eruptive epochs. Moreover, the overall asymmetric topography of the caldera, with the highest relief along its northeast rim (200–300 m above sea level) and the lowest bathymetry in the southern part (50–100 m below sea level), explains also the asymmetric distribution of vents, which cluster in the currently onshore northeast part. In fact, any magma lens below the central portion of the caldera tends to be attracted by the zone of highest relief, where the deviatoric stress is highest, thus propagating towards that direction. The reconstructed evolution of the stress distribution at Campi Flegrei has allowed not only explaining the vent distribution in the last 15 ka, but also hindsight forecasting of the location of the last 1538 Monte Nuovo vent. This in fact lies in the onland annular portion, at ~3 km from the caldera centre, which is also the most likely location for the opening of future vents (Rivalta et al. 2019). A consistent relationship between the location of vents and the stress distribution is observed also at other calderas with known eruptive history and overall stress state, suggesting a wider applicability of the approach, including the possibility to forecast the location of vents (Fig. 5.22). This method may provide an important advancement in building physics-based hazards maps of the probability of opening of a vent at a volcano. In fact, current hazards maps are typically description-based (considering only the location of the past vents, without explaining their distribution with physical models), resulting in limited forecast.

While the concept of stress unloading may generally explain the shallow transfer of magma and opening of vents feeding the minor eruptions commonly observed at calderas, it may be less applicable to the less frequent caldera-forming eruptions, where the rise of magma with higher pressure and buoyancy may be less affected by the unloading stress distribution (see also Sect. 7.5).

5.10 Lessons from Active Calderas

As introduced, calderas are the most active type of volcano, characterized by long-term resurgence, short-term unrest and eruptions of any size, with exclusive pertinence of the largest sizes. Active calderas have shown remarkable examples of these types of activity in the last decades, permitting to better understand their behaviour and processes. This section summarizes some relevant events, considering unrest

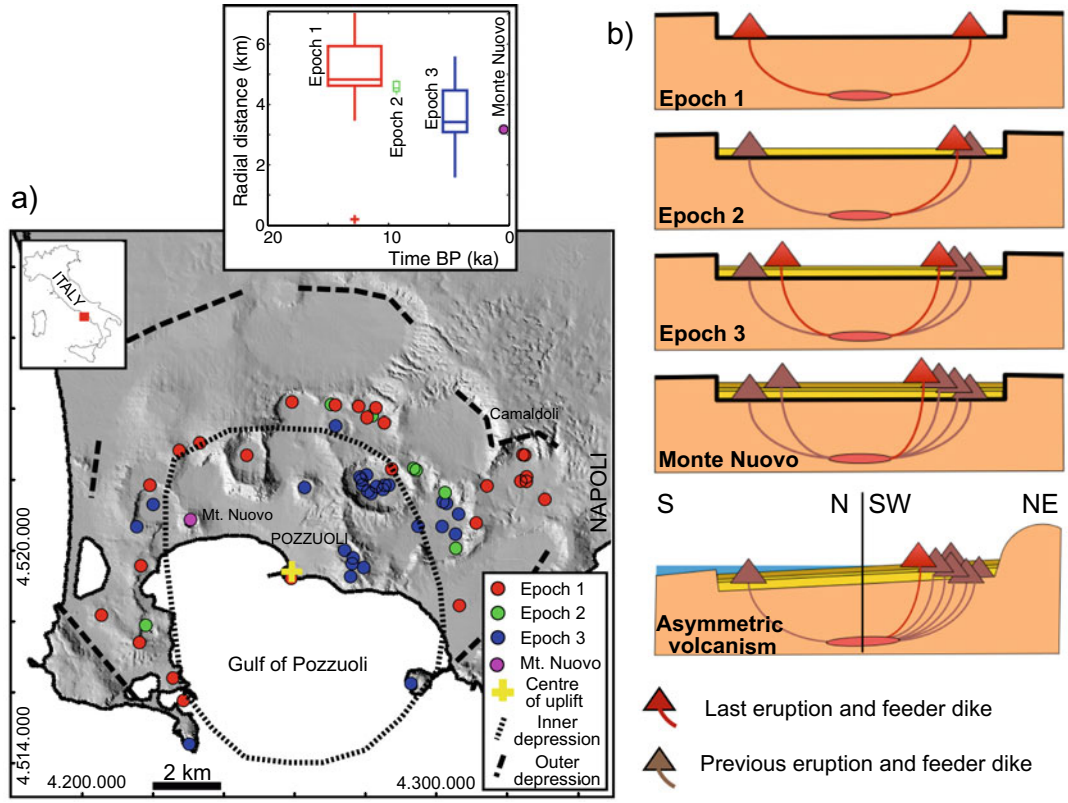

Fig. 5.21 **a** Distribution of the post-caldera vents (coloured circles) at Campi Flegrei as a function of its three epochs of eruptive activity; volcanism migrates inward with time (upper inset), clustering in the northeast part of the caldera. **b** This eruptive pattern results from the progressive thickening of the marine and volcanic infill within the caldera (yellow), which gradually shifts the location of the eruptive vents (triangles) inward. Also, the asymmetric distribution of the vents is explained by the highest relief to the northeast, which develops stronger gravitational loads and thus attracts magma (bottom diagram; modified after Acocella and Rivalta 2019)

culminating in eruption (eruptive unrest) from mafic and felsic calderas, as well as episodes of caldera collapse.

5.10.1 Sierra Negra

Eruptive unrest recently occurred at both mafic and felsic calderas. Among mafic calderas, the unrest predating the 2005 eruption at Sierra Negra shows several interesting features. Sierra Negra is the most voluminous volcano in the western Galapagos Archipelago. Above sea level, it is 60 × 40 km wide and 1140 m high, with a summit caldera larger (7 × 10 km) but shallower (110 m deep) than the other calderas in the western Galapagos. More than ten historical eruptions have occurred since 1813, producing lava flows on the north flank. InSAR results from three different intervals between 1992 and 1999 showed that the caldera floor inflated by 2.7 m. From 1992 to 1997, the inflation pattern was nearly axisymmetric to the caldera centre: this was modelled as due to the intrusion of magma into a sill beneath the caldera, at 2 km of depth. Between 1997 and 1998 the maximum uplift, consisting of ~1.2 m of slip along a steeply south-dipping normal fault, was centred on the southern limb of a pre-existing intracaldera fault system. The focus of inflation shifted back to the caldera centre between 1998 and 1999, again interpreted as magma filling a sill (Fig. 5.23;

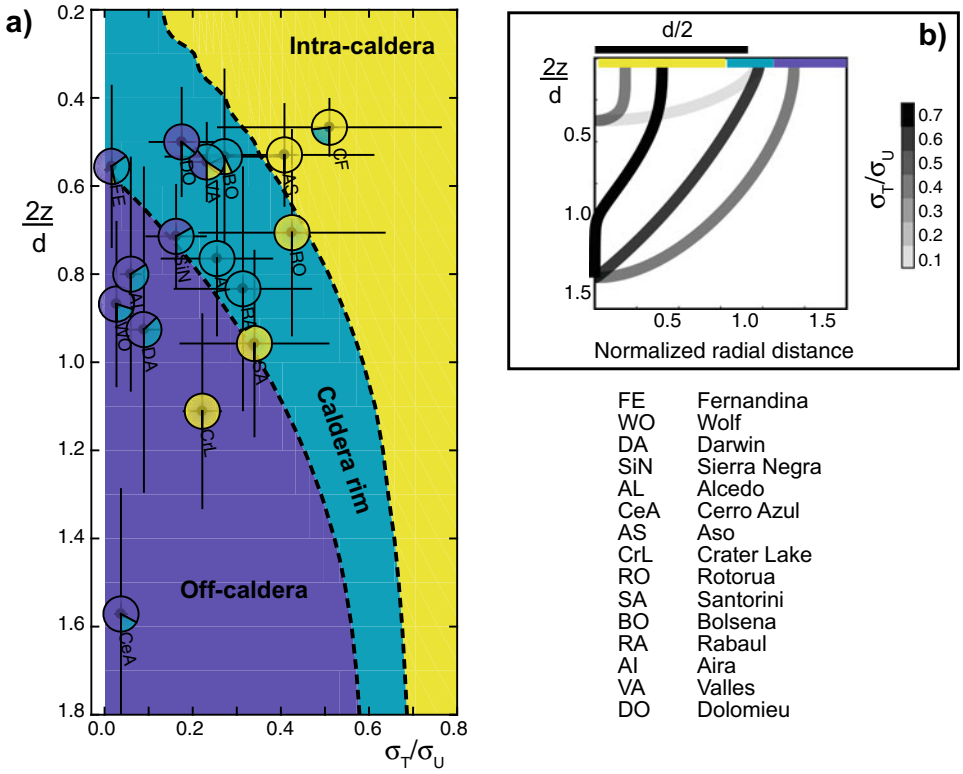

Fig. 5.22 **a** Application of the unloading model to several calderas worldwide (listed to the bottom right). The background colours represent the domain for the predicted location of the intra-caldera, caldera rim, and off-caldera vent locations as a function of the ratio between the depth to the magma chamber z and the caldera radius $d/2$, that is $2z/d$, and the ratio between the tectonic σ_T and unloading stress σ_U, that is σ_T/σ_U. Estimates for calderas in nature are represented by pie plots according to the proportion of observed intra-caldera, rim, or off-caldera vents, with the same colour coding as the background. Uncertainties are shown as black lines. The overall agreement (except for Crater Lake and Santorini) between the predicted and observed vent patterns suggests a broad control of unloading on shallow magma transfer at calderas. **b** Examples of streamlines of selected models with $2z/d = 0.4$ and $2z/d = 1.4$ and variable σ_T/σ_U, which controls trajectory concavity (modified after Rivalta et al. 2019)

Amelung et al. 2000; Jonsson et al. 2005). GPS data during 2000–2003 showed a deceleration in the uplift rate, followed by a change to subsidence of 9 cm/year. The deflationary source was modelled as a contracting sill at a depth of 2.1 km, similar to the inflationary source of the 1990s. In April 2003, deformation of the caldera floor reversed to inflation. The inflation rate gradually increased throughout 2004 and into 2005, for a total uplift of 89 cm, accompanied by 69 cm of horizontal extension across the caldera. Inflation was interrupted by an episode of inelastic trapdoor faulting, marked by a magnitude *M4.6* earthquake on 16 April 2005. This produced 84 cm of uplift on the southern part of the caldera and contraction of the cross-caldera line by 26 cm. Modelling results for this trapdoor faulting suggest slip on a high angle inward dipping reverse fault, extending from the surface down to the sill at 2.2 km depth (Fig. 5.23).

The inflation rate was not affected by this faulting event, approaching 1 cm/day. Parts of the caldera uplifted of 1.22 m between the faulting event and a successive *M5.4* earthquake on 22 October 2005, probably occurred again along the faults in the southern part of the

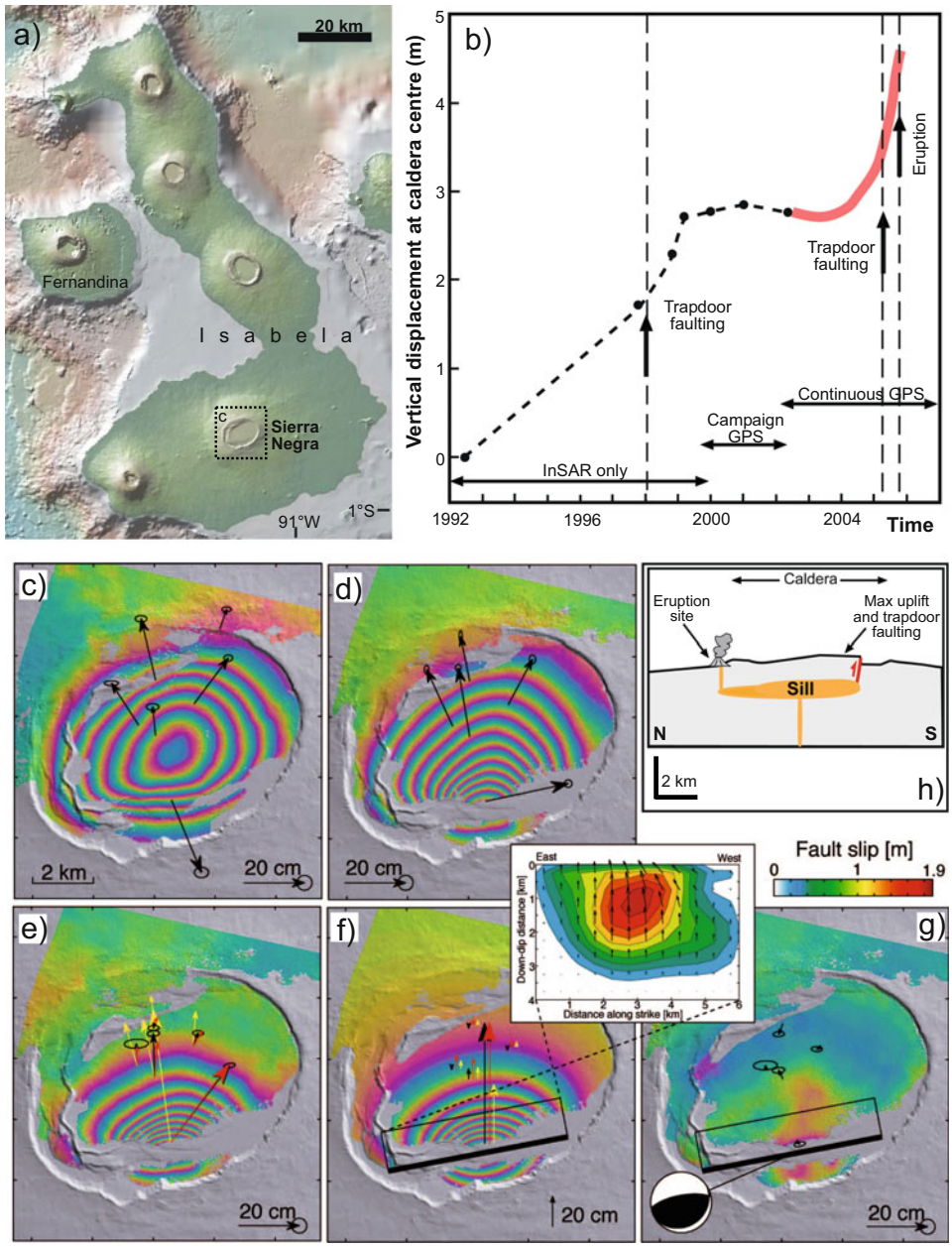

Fig. 5.23 Unrest and eruption at Sierra Negra caldera, Galapagos. **a** Location of Sierra Negra caldera. **b** Vertical displacement of caldera floor from 1992 to 2005, culminating in the 2005 eruption, detected through geodetic data. **c–g** InSAR and GPS data and comparison with trapdoor fault models: **c** uplift from February 12, 2004 to January 27, 2005; InSAR displacement is 10 cm per fringe; **d** uplift and trapdoor faulting from January 27, 2005 to May 12, 2005; **e** same as **d**, but corrected for deformation due to uplift and effectively only showing deformation due to trapdoor faulting on April 16, 2005; black and red vectors show observed and predicted horizontal displacements, respectively; yellow vectors in (**e**) and (**f**) show predicted displacements from previous models; **f** simulated interferogram from trapdoor fault model (inset); **g** residual between **e** and **f**; focal mechanism shows modelled sense of slip (after Chadwick et al. 2006). **h** Section view diagram summarizes the relationships between sill emplacement beneath the caldera, trapdoor faulting on the south side and eruptions on the north flank (after Jonsson et al. 2005)

caldera. The static stress transfer induced by the latter earthquake may have triggered tensile failure and catalysed the onset of the eruption three hours later (Gregg et al. 2018). The eruption, responsible for a 13 km high steam and ash plume, opened a fissure inside the north rim, on the opposite side with regard to the location of the *M4.6* and *M5.4* events, feeding a total eruptive volume of $\sim 150 \times 10^6$ m^3. From 1 April 2003 to 22 October 2005, at the eruption onset, the precursory maximum uplift reached $\sim$2.2 m, bringing the total amount of uplift since 1992 to nearly 5 m (Chadwick et al. 2006). Conversely, during the 8 days of the eruption, the caldera floor deflated $\sim$5 m and the volcano contracted horizontally $\sim$ 6 m (Geist et al. 2008).

This eruptive unrest has been characterized by the largest, although discontinuous, precursory inflation ($\sim$5 m) ever recorded at a mafic caldera. In addition, it shows two interesting features. First, the eruptive vent was located on the opposite side with regard to the most uplifted area, where the earthquakes were also detected. This is explained by the fact that the trapdoor faulting due to the *M4.6* and *M5.4* earthquakes relieved the pressure within the sill to the south, at the same time inducing compression south of the fault and inhibiting the lateral propagation of the sill. As a result, the sill thickened on this side, postponing any eruption. However, the faulting also caused a radially directed tension on the opposite side of the caldera, encouraging circumferential dike propagation at the northern periphery of the sill, finally feeding the eruption (Jonsson 2009). A second feature is the seismogenic reactivation of the reverse fault characterizing the trapdoor uplift, during the *M4.6* event. This fault borders the southern and most uplifted portion of the $\sim$100 m high tilted resurgent block of Sierra Negra. This pre-eruptive trapdoor uplift may thus constitute an episode of growth of the longer-term resurgence, similarly to what observed at the nearby Alcedo caldera during the 2007–2011 non-eruptive inflation, where a fault bordering the minor resurgent block was reactivated (Galetto et al. 2019). The consistency in the shorter- and longer-term deformation pattern at these mafic calderas supports the possibility that resurgence results from cumulated and distinct unrest episodes.

5.10.2 Rabaul

Rabaul caldera (Papua New Guinea) is one of the most active felsic calderas. It consists of a pair of elongated nested collapse structures, the inner being identified by focused seismicity along high-angle outward dipping faults (Fig. 5.24). Rabaul produced several caldera-forming eruptions: after the last, in AD 640, more than 8 intracaldera eruptions have been occurring. The last three eruptions (1878, 1937–1941 and between 1994-Present) showed the simultaneous activity of the Tavurvur (andesitic-dacitic) and Vulcan (dacitic-andesitic) eruptive centres, lying on opposite sides along the inner, active caldera (Mori and McKee 1987; Nairn et al. 1995). Rabaul experienced several unrest episodes, culminating in an eruption sequence starting in 1994 (Fig. 5.24). Following two nearby *M8* tectonic earthquakes in 1971, Rabaul experienced progressive uplift and shallow seismicity (less than 3 km of depth) along the inner ring-fault. Between 1971 and 1983, thousands of earthquakes were accompanied by a cumulative uplift of 1 m. In 1983, both the seismicity and uplift rate dramatically increased, possibly following a *M7.6* regional earthquake 200 km to the east. This phase lasted until July 1985 and was characterized by several tens of thousands of earthquakes and uplift of $\sim$1 m. The 1983–1985 unrest phase has been interpreted as due to the injection of mafic magma. From August 1985 to April 1992 the seismicity and uplift rate significantly decreased. From May 1992 to September 1994, the uplift and seismicity rate increased again, although with a much lower rate than that observed between 1983 and 1985. A burst of seismicity occurred on Late August 1994, followed by quiescence until September 18, when a *M5.1* earthquake occurred at a depth of 1.2 km in

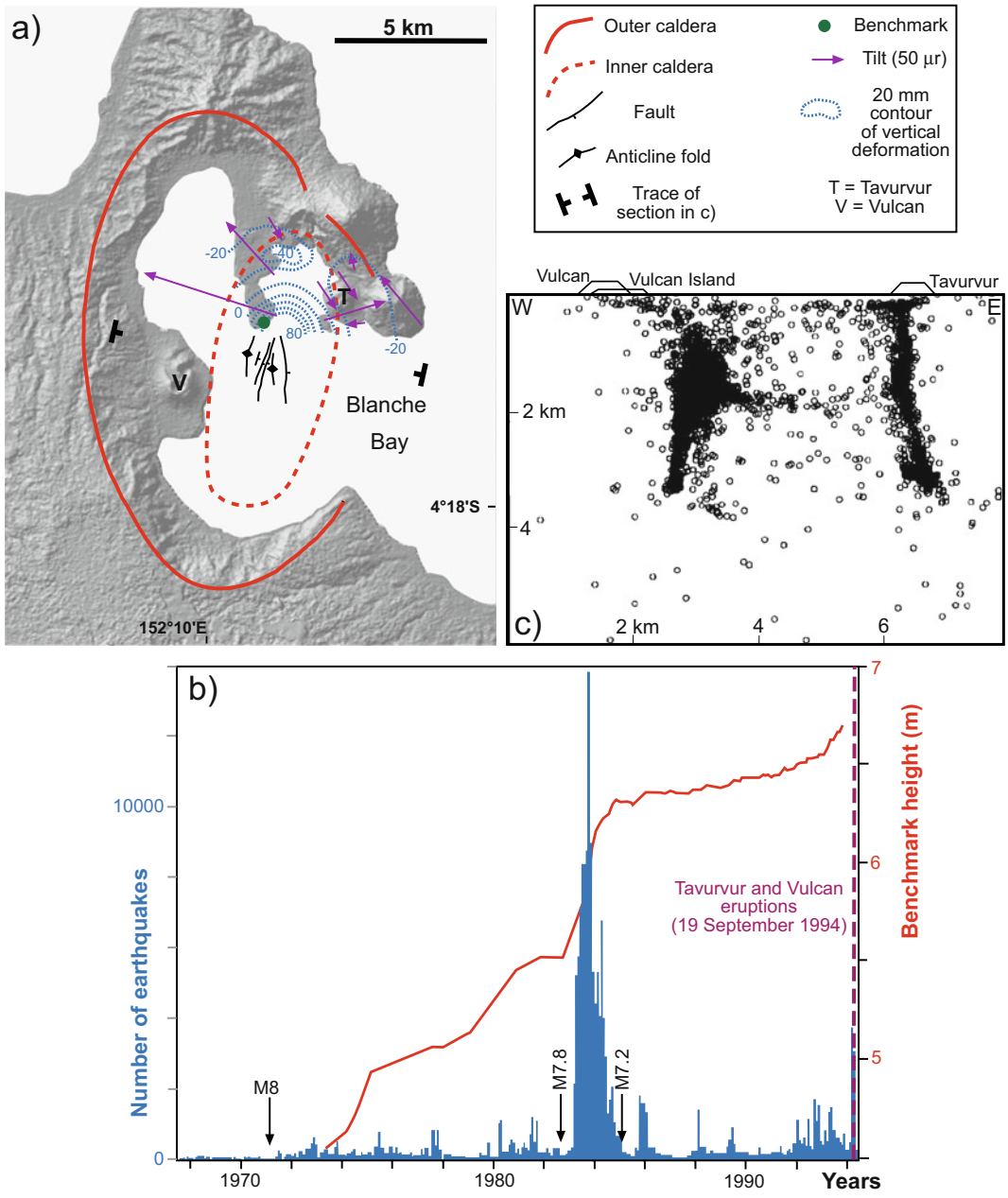

Fig. 5.24 Unrest and eruption at Rabaul caldera (Papua New Guinea). **a** Simplified structure, showing the two nested collapses and the deformation between 7/85 and 9/89, highlighted by the uplift contours, the tilt data and faults and folds (modified after Saunders 2001). **b** Monthly total earthquakes (blue histogram) and compounded uplift (red line) between 1968 and 1994; nearby major regional earthquakes are also indicated (modified after Johnson et al. 2010). **c** Approximately E-W-trending section (location in **a**) showing the projection of the seismicity in the central portion of the caldera between 1971 and 1992, with the seismicity clustering along outward dipping faults; the projection of Vulcan and Tavurvur vents is also included (modified after Jones and Stewart 1997)

the eastern part of the caldera. After only 27 h of sustained seismicity, 12 of which included low-frequency events, the eruption begun on September 19. Tavurvur, on the east rim, erupted first, immediately preceded by an uplift of 1–2 m. Approximately 1–1.5 h later Vulcan, following a localized uplift of 6 m also starting a few hours before the eruption, erupted from at least 4 vents. Several tsunamis were generated during the onset of the eruption. Soon after the eruption onset, the caldera deflated. The initial part of the VEI 4 eruption was the most violent, generating an ash cloud ~20 km high. Vulcan's eruption ended on 2 October, while the eruption at Tavurvur, after peaking during the first five days of activity, lasted until April. At the end of October, the subsidence of the caldera reached 1 m in the central part and 20–30 cm along the rim. Seismic activity along the caldera rim progressively decreased from the beginning of October to the end of November. At least 5 other explosive eruptive events, with VEI between 1 and 4, occurred from November 1995 to July 2010 (Johnson et al. 2010).

The 1971–1994 eruptive unrest at Rabaul shows several interesting features. First, higher seismicity and uplift between 1983 and 1985 were not immediately followed by any eruption, while moderate seismicity and uplift occurring between 1992 and 1994 culminated in a VEI 4 eruption. This behaviour may be understood only by considering the second phase as a continuation and dependent on the first: the first primed the system and the second set off the eruption (Acocella et al. 2015; Robertson and Kilburn 2016). Second, in at least two cases, in 1971 and 1983, the unrest of the caldera, or its intensification, occurred immediately after major regional earthquakes, suggesting interactions between tectonic events and a prepared magmatic reservoir. However, while Rabaul responded to a *M7* earthquake at a distance of 180 km with a pronounced earthquake swarm, it did not produce any detectable activity in response to a second *M7* earthquake two months later, at a distance of only 60 km (Johnson et al. 2010). Another remarkable feature is the simultaneous activation of two vents along opposite portions of the caldera ring fault. This feature has been also demonstrated for the 4.3 ka Solfatara and Averno eruptions at Campi Flegrei, fed by two vents within the caldera erupting products with different compositions (Pistolesi et al. 2016).

5.10.3 Recent Caldera Collapses

In addition to eruptions, calderas experience collapse episodes. Seven episodes of caldera collapse have been observed and/or monitored in the last decades: Fernandina (1968, Galapagos), Pinatubo (1991, Philippines), Miyakejima (2000, Japan), Dolomieu (2007, La Réunion), Bardarbunga (2014, Iceland), Axial Seamount (2015, Juan de Fuca Ridge) and Kilauea (2018, Hawaii). In addition, a more limited subsidence (2.5 m) has been detected at Ambrym caldera (2018; Vanuatu; Stix and Kobayashi 2008; Michon et al. 2011; Gudmundsson et al. 2016; Wilcox et al. 2016; Neal et al. 2019; Shreve et al. 2019). All these episodes were related to eruptions, although their size differed significantly, from minor eruptions, as the VEI 1 eruption at Dolomieu in 2007, to major eruptions, as the VEI 6 Pinatubo eruption in 1991. Also, with the exception of Pinatubo, all these collapses occurred with mafic magma. These episodes, especially the best-monitored later ones, have provided a wealth of valuable information to better understand the mechanism of collapse and its triggering factors.

As far as the mechanism of collapse is concerned, geodetic and seismicity observations at Miyakejima, Dolomieu, Bardarbunga and Kilauea have revealed a common step-by-step, incremental mode of collapse unfolding over days, weeks or months (e.g. Michon et al. 2011; Gudmundsson et al. 2016; Munekane et al. 2016; Neal et al. 2019). This can be mechanically described in simple terms by the vertical slip of a cylindrical piston driven by gravity and resisted by friction on the ring slip surface and by the rebound force exerted by the compressible magma onto the sliding piston (Kumagai et al. 2001). Both the 2007 Dolomieu and the 2018

Kilauea collapse showed a reduction of the time-interval between successive subsidence increments, which resulted from the acceleration of magma withdrawal and a progressive weakening of the edifice at the beginning of the sequence (Duputel and Rivera 2019). Where the caldera faults were not completely reactivated, because of the lower amount of collapse, the seismicity along the caldera ring faults was limited. This was the case of Bardarbunga in 2014, where caldera subsidence was largely aseismic, with seismicity accounting for 10% or less of the geodetic moment. Approximately 90% of the seismic moment release occurred on the most subsided northern rim, highlighting asymmetric collapse (Agustdottir et al. 2019).

As for the triggering factors, with the exception of the largest felsic eruption occurring at the summit of Pinatubo, all the remaining caldera collapse episodes, including the subsidence at Ambrym, were related to the withdrawal of the magma chamber induced by the lateral migration of dikes, eventually erupting outside the caldera. In some cases, as at Bardarbunga in 2014 and Kilauea in 2018, the eruption occurred downslope along the rift zone, 40–50 km away. This similarity among most collapse episodes highlights the importance of the lateral intrusion of magma in generating collapse at mafic calderas, even though the same process may show distinct features, in terms of amount and mode of collapse, distance of vents and eruptive activity (Sigmundsson 2019). At Bardarbunga, observations highlight an exponential decline of the magma flow rate at the eruption site at the tip of the laterally propagating dike, coupled with the exponential rate of volume change in the caldera, consistently with theoretical predictions (see also Sect. 4.6.3; Gudmundsson et al. 2016). The 2018 Kilauea collapse allowed clarifying in more detail the possible conditions that trigger the onset of collapse, as well as those controlling the eruptive flow (Fig. 5.25). At Kilauea failure began after less than 4% of magma was withdrawn from a shallow reservoir beneath the volcano's summit. Also, several cubic kilometres of magma were stored in the reservoir, and only a fraction was withdrawn before the end of the

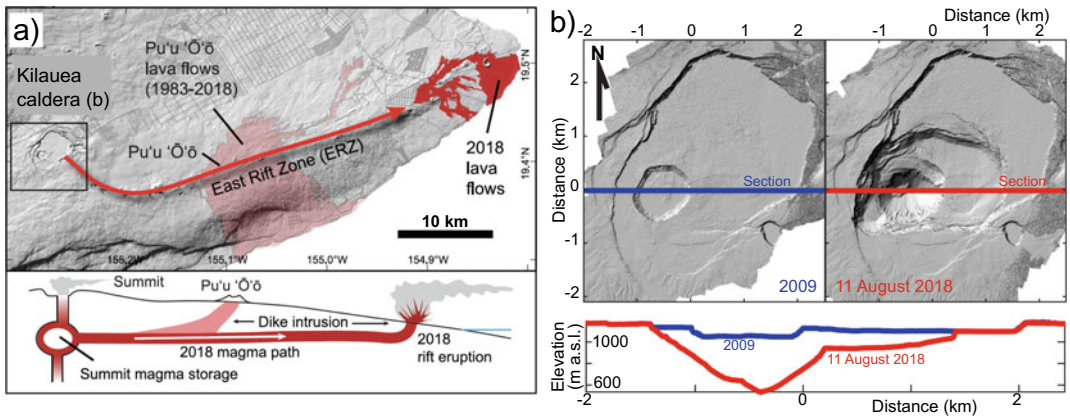

Fig. 5.25 Kilauea Volcano (Hawaii, USA) and the 2018 eruption. **a** During the eruption, magma flowed for more than 40 km underground subhorizontally from the summit (left) to the lower Eastern Rift Zone (ERZ) vents (above). Schematic cross section (not to scale) showing flow of magma from the summit to the lower ERZ (below; modified after Anderson et al. 2019). **b** Digital elevation models of Kilauea's summit from 2009 (left) and 11 August 2018 (right), highlighting the collapse of the caldera. The red and blue lines correspond to the locations of the cross sections shown at the bottom. The difference between the 2009 and 2018 profiles gives the amount of subsidence that occurred almost entirely since 1 May 2018 (images courtesy of Kyle Anderson and Christina Neal, USGS; modified after Neal et al. 2019)

eruption. This indicates that, in presence of a shallow reservoir, caldera formation may begin after withdrawal of only small amounts of magma, and may end well before source reservoirs are completely evacuated. In addition, episodic fault-bounded subsidence of the roof block above the reservoir increased magma pressure, sustaining the lateral flow of magma. Therefore, the collapsing block also drove out a large volume of magma as it subsided. This feature was supported by observations at the main vent along the rift zone, which exhibited cyclic eruption rates on long (tens of hours) time scales, due to pressure-driven surges in magma supply triggered by summit caldera collapse events 40 km upslope. Such a connection between the summit magma reservoir and the flank eruption allowed the episodic nature of summit collapses to be rapidly expressed as changes in eruption vigour on the flank (Anderson et al. 2019; Patrick et al. 2019).

5.11 Summary

Calderas are the most active yet challenging type of volcano. Caldera collapse may occur in very different conditions, most commonly during lateral intrusion of magma from mafic chambers and less often following large explosive eruptions from felsic chambers. Even though several differences exist in the collapse of mafic and felsic calderas, the mechanism, structure and evolutionary stages of collapse are the same and depend upon the amount of subsidence s with regard to the caldera diameter d, or the s/d ratio. This ratio allows defining four stages of collapse, with distinct deformation pattern, experienced by calderas.

Calderas sometimes experience longer-term uplift of their floor, or resurgence, which develops blocks or domes. Resurgence is the surface expression of the repeated shallow emplacement of new magma, unable to reach the surface and erupt because of the relatively low-viscosity contrast with the residual magma. On the shorter-term, caldera activity is often characterized by deformation, seismicity and degassing, highlighting unrest, which usually results from the shallow emplacement of magma. Comparison between the shorter-term unrest and longer-term resurgence suggests a connection, with resurgence likely resulting from the cumulative net uplift produced by multiple unrest episodes. Therefore, uplift during unrest at a resurgent caldera may be the short-term expression of resurgence.

The accumulated magma during resurgence and unrest may be finally transferred, eventually leading to eruption. For a given caldera diameter, the amount of subsidence of the caldera, albeit corrected for the presence of any infill, controls the shallow propagation path of magma. In fact, the mass removal due to the development of the caldera depression determines the local unloading stress. This, in addition to regional stresses and magma buoyancy, explains the propagation path of dikes and the distribution of eruptive vents at several calderas, and may also allow forecasting the location of future vents, as proposed for Campi Flegrei and other calderas. Nevertheless, the propagation of dikes feeding caldera-forming eruptions, as associated with magma with higher pressure and buoyancy, may be less affected by the unloading stresses.

5.12 Main Symbols Used

A_r	aspect ratio
d	caldera diameter
L	width of crust overlying the magma chamber
M	magnitude
s	caldera subsidence
z	depth of crust overlying the magma chamber
σ_1	maximum principal stress
σ_3	minimum principal stress
σ_M	maximum horizontal principal stress
σ_m	minimum horizontal principal stress

References

Acocella V, Cifelli F, Funiciello R (2001) The control of overburden thickness on resurgent domes: insights from analogue models. J Volcanol Geoth Res 111:137–153

Acocella V (2007) Understanding caldera structure and development: an overview of analogue models compared to natural calderas. Earth-Sci Rev 85:125–160

Acocella V (2010) Coupling volcanism and tectonics along divergent boundaries: collapsed rifts from Central Afar, Ethiopia. Geol Soc Am Bull 122:1717–1728

Acocella V, Palladino DM, Cioni R, Russo P, Simei S (2012) Caldera structure, amount of collapse and erupted volumes: the case of Bolsena Caldera, Italy. Geol Soc Am Bull 124:1562–1576

Acocella V, Di Lorenzo R, Newhall C, Scandone R (2015) An overview of recent (1988 to 2014) caldera unrest: knowledge and perspectives. Rev Geophys 53. https://doi.org/10.1002/2015RG000492

Acocella V (2019) Bridging the gap from caldera unrest to resurgence. Front Earth Sci 7:173. https://doi.org/10.3389/feart.2019.00173

Acocella V, Rivalta E (2019) Calderas: structure, unrest, magma transfer and eruptions. Reference module in earth systems and environmental sciences. Elsevier 15 p

Aguirre-Diaz GJ, Labarthe-Hernandez G, Tristan-Gonzalez M, Nieto-Obregon J, Gutierrez-Palomares I (2008) The ignimbrite flare-up and graben calderas of the Sierra Madre Occidental, Mexico. In: Marti J, Gottsmann J (eds) Caldera volcanism: analysis, modelling and response: developments in volcanology. Elsevier, vol 10, pp 285–311

Agustsdottir T, Winder T, Woods J, White RS, Greenfield T, Brandsdottir B (2019) Intense seismicity during the 2014–2015 Bardarbunga-Holuhraun rifting event, Iceland, reveals the nature of dike-induced earthquakes and caldera collapse mechanisms. J Geophys Res 124:8331–8357

Amelung F, Jonsson S, Zebker H, Segall P (2000) Widespread uplift and 'trapdoor' faulting on Galapagos volcanoes observed with radar interferometry. Nature 407:993–996

Amoruso A, Crescentini L, D'Antonio M, Acocella V (2017) Thermally-assisted magma emplacement explains restless calderas. Sci Rep 7:7948. https://doi.org/10.1038/s41598-017-08638-y

Anderson KR, Johanson IA, Patrick MR, Gu M, Segall P, Poland MP et al (2019) Magma reservoir failure and the onset of caldera collapse at Kīlauea Volcano in 2018. Sci 366:eaaz1822

Bagnardi M, Amelung F, Poland MP (2013) A new model for the growth of basaltic shields based on deformation of Fernandina volcano, Galápagos Islands. Earth Planet Sci Lett 377–378:358–366

Bathke H, Nikkhoo M, Holohan EP, Walter TR (2015) Insights into the 3D architecture of an active caldera ring-fault at Tendürek volcano through modeling of geodetic data. Earth Planet Sci Lett 422:157–168

Bosworth W, Burke K, Strecker M (2003) Effect of stress fields on magma chamber stability and the formation of collapse calderas. Tectonics 22:1042. https://doi.org/10.1029/2002TC001369

Branney M, Acocella V (2015) Calderas. In: Sigurdsson H, Houghton B, Rymer H, Stix J (eds) The encyclopaedia of volcanoes, 2nd edn. Academic Press, pp 299–315

Cabaniss HE, Gregg PM, Grosfils EB (2018) The role of tectonic stress in triggering large silicic caldera eruptions. Geophys Res Lett 45:3889–3895

Chadwick WW, Howard KA (1991) The pattern of circumferential and radial eruptive fissures on the volcanoes of Fernandina and Isabela islands, Galapagos. Bull Volcanol 53:259–275

Chadwick WW, Geist DJ, Jonsson S, Poland M, Johnson DJ, Meertens CM (2006) A volcano bursting at the seams: inflation, faulting, and eruption at Sierra Negra volcano, Galápagos. Geology 34:1025–1028

Chang W-L, Smith RB, Wicks C, Farrell JM, Puskas CM (2007) Accelerated uplift and magmatic intrusion of the yellowstone Caldera, 2004 to 2006. Science 318:952. https://doi.org/10.1126/science.1146842

Chen JK, Taylor FW, Edwards RL, Cheng H, Burr GS (1995) Recent emerged reef terraces of the Yenkahe resurgent block, Tanna, Vanuatu: implications for volcanic, landslide and tsunami hazards. J Geol 103:577–590

Chesner CA (2012) The Toba caldera complex. Quatern Int 258:5–18

Christiansen RL (2001) The quaternary and pliocene yellowstone plateau volcanic field of Wyoming, Idaho, and Montana. U.S. Geological Survey Professional Paper 729-G:120 pp

Clague DA, Paduan JB, Caress DW, Moyer CL, Glazer BT, Yoerger DR (2019) Structure of Loihi Seamount, Hawai'i and Lava Flow morphology from high-resolution mapping. Front Earth Sci 7:58. https://doi.org/10.3389/feart.2019.00058

Cole JW, Milner DM, Spinks KD (2005) Calderas and caldera structures: a review. Earth-Sci Rev 69:1–96

Coleman DS, Mills RD, Zimmerer RJ (2016) The pace of plutonism. Elements 12:97–102

Corbi F, Rivalta E, Pinel V, Maccaferri F, Bagnardi M, Acocella V (2015) How caldera collapse shapes the shallow emplacement and transfer of magma in active volcanoes. Earth Planet Sci Lett 431:287–293

De Chabalier JB, Avouac JP (1994) Kinematics of the Asal Rift (Djibouti) determined from the deformation of Fieale Volcano. Science 265:1677–1681

De Natale G, Pingue F (1993) Ground deformation in collapsed calderas structures. J Volcanol Geoth Res 57:19–38

De Saint Blanquat M, Horsman E, Habert G, Morgan S, Vanderhaeghe O, Law R et al (2011) Multiscale magmatic cyclicity, duration of pluton construction, and the paradoxical relationship between tectonism

and plutonism in continental arcs. Tectonophysics 500:20–33
de Silva SL, Mucek AE, Gregg PM, Pratomo I (2015) Resurgent Toba—field, chronologic, and model constraints on duration, time scales and mechanisms of resurgence at large calderas. Front Earth Sci 3. https://doi.org/10.3389/feart.2015.00025
Delgado F, Pavez A (2015) New insights into La Pacana caldera inner structure based on a gravimetric study (central Andes, Chile). Andean Geol 42:313–328
Di Vito MA, Isaia R, Orsi G, de Vita S, D'Antonio M, Pappalardo L et al (1999) Volcanism and deformation since 12000 years at the Campi Flegrei caldera (Italy). J Volcanol Geoth Res 91:221–246
Di Vito MA, Acocella V, Aiello G, Barra D, Battaglia M, Carandente A et al (2016) Magma transfer at Campi Flegrei caldera (Italy) before the last 1538 AD eruption. Sci Rep 6:32245. https://doi.org/10.1038/srep32245
Druitt T, Spark RSJ (1984) On the formation of calderas during ignimbrite eruptions. Nature 310:679–681
Duputel Z, Rivera L (2019) The 2007 caldera collapse of Piton de la Fournaise volcano: source process from very-long-period seismic signals. Earth Planet Sci Lett 527:115786
Dvorak JJ, Dzurisin DD (1997) Volcano geodesy: the search for magma reservoirs and the formation of eruptive vents. Rev Geophys 35:343–384
Farrell J, Smith RB, Husen DT (2014) Tomography from 26 years of seismicity revealing that the S. spatial extent of the Yellowstone crustal magma reservoir extends well beyond the Yellowstone caldera. Geophys Res Lett 41:3068–3073
Fridrich CJ, Smith RP, De Witt ED, McKee EH (1991) Structural, eruptive and intrusive evolution of the grizzly peak caldera, Sawatch Range, Colorado. Geol Soc Am Bull 103:1160–1177
Gaete A, Kavanagh JL, Rivalta E, Hazimb SH, Walter TR, Dennis DJC (2019) The impact of unloading stresses on post-caldera magma intrusions. Earth Planet Sci Lett 508:109–121
Galetto F, Acocella V, Caricchi L (2017) Caldera resurgence driven by magma viscosity contrasts. Nat Commun 8:1750. https://doi.org/10.1038/s41467-017-01632-y
Galetto F, Bagnardi M, Acocella V, Hooper A (2019) Noneruptive unrest at the caldera of Alcedo Volcano (Galápagos Islands) revealed by InSAR data and geodetic modelling. J Geophys Res 124. https://doi.org/10.1029/2018JB017103
Garden TO, Chambefort I, Gravley DM, Deering CD, Kennedy BM (2020) Reconstruction of the fossil hydrothermal system at Lake City caldera, Colorado, U.S.A.: constraints for caldera-hosted geothermal systems. J Volcanol Geotherm Res 393:106794
Genrich JF, Bock Y, McCaffrey R, Prawirodirdjo L, Stevens CW, Puntodewo SSO et al (2000) Distribution of slip at the northern Sumatran fault system. J Geophys Res 105:28327–28341
Geshi N, Shimano T, Chiba T, Nakada S (2002) Caldera collapse during the 2000 eruption of Miyakejima volcano, Japan. Bull Volcanol 64:55–68
Geyer A, Folch A, Martì J (2006) Relationship between caldera collapse and magma chamber withdrawal: an experimental approach. J Volcanol Geoth Res 157:375–386
Geyer A, Martì J (2014) A short review of our current understanding of the development of ring faults during collapse caldera formation. Front Earth Sci 2. https://doi.org/10.3389/feart.2014.00022
Glazner AF, Bartley JM, Coleman D, Gray W, Taylor RZ (2004) Are plutons assembled over millions of years by amalgamation from small magma chambers? GSA Today 14. https://doi.org/10.1130/1052-5173
Goto I, McPhie J (2018) Tectonics, structure, and resurgence of the largest Quaternary caldera in Japan: Kutcharo, Hokkaido. Geol Soc Am Bull 130:1307–1322
Gregg P, de Silva SL, Grosfils EB, Parmigiani JP (2012) Catastrophic caldera-forming eruptions: thermomechanics and implications for eruption triggering and maximum caldera dimensions on Earth. J Volcanol Geoth Res 241–242:1–12
Gregg PM, Le Mével H, Zhan Y, Dufek J, Geist D, Chadwick WW (2018) Stress triggering of the 2005 eruption of Sierra Negra volcano, Galápagos. Geophys Res Lett 45:13288–13297
Gudmundsson MT, Jónsdóttir K, Hooper A, Holohan EP, Halldórsson SA, Ófeigsson BG et al (2016) Gradual caldera collapse at Bárdarbunga volcano, Iceland, regulated by lateral magma outflow. Science 353 (6296): aaf8988
Gudmundsson A (1998) Formation and development of normal fault calderas and the initiation of large explosive eruptions. Bull Volcanol 60:160–170
Gudmundsson A (2007) Conceptual and numerical models of ring-fault formation. J Volcanol Geoth Res 164:142–160
Han R, Kim J-S, Kim C-M, Hirose T, Jeong JO, Jeon GY (2019) Dynamic weakening of ring faults and catastrophic caldera collapses. Geology 47:107–110
Hardy S (2008) Structural evolution of calderas: Insights from two-dimensional discrete element simulations. Geology 36:927–930
Harris AJL (2009) The pit-craters and pit-crater-filling lavas of Masaya volcano. Bull Volcanol 71:541–558
Hildreth W, Fiersetin J, Calvert A (2017) Early postcaldera rhyolite and structural resurgence at Long Valley Caldera, California. J Volcanol Geoth Res 335:1–34
Holohan EP, Troll VR, Walter TR, Munn S, McDonnell S, Shipton ZK (2005) Elliptical calderas in active tectonic settings: an experimental approach. J Volcanol Geoth Res 144:119–135
Holohan EP, Troll VR, van Wyk deVries B, Walsh JJ, Walter TR, (2008) Unzipping long valley: an explanation for vent migration patterns during an elliptical ring fracture eruption. Geology 36:323–326
Holohan EP, Schopfer MPJ, Walsh JJ (2011) Mechanical and geometric controls on the structural evolution of

pit crater and caldera subsidence. J Geophys Res 116: B07202. https://doi.org/10.1029/2010JB008032
Hotovec-Ellis AJ, Shelly DR, Hill DP, Pitt AM, Dawson PB, Chouet BA (2018) Deep fluid pathways beneath Mammoth Mountain, California, illuminated by migrating earthquake swarms. Sci Adv 4: eaat5258
Isaia R, Vitale S, Marturano A, Aiello G, Barra D, Ciarcia S et al (2019) High-resolution geological investigations to reconstruct the long-term ground movements in the last 15 kyr at Campi Flegrei caldera (southern Italy). J Volcanol Geoth Res 385:143–158
Jellinek AM, DePaolo DJ (2003) A model for the origin of large silicic magma chambers: precursors of caldera-forming eruptions. Bull Volcanol 65:363–381
Jiang C, Schmandt B, Farrell J, Lin F-C, Ward KM (2018) Seismically anisotropic magma reservoirs underlying silicic Calderas. Geology 46:727–730
Johnson R, Itikarai I, Patia H, McKee C (2010) Volcanic systems of the Northeastern Gazelle Peninsula, Papua New Guinea: Synopsis, evaluation, and a model for Rabaul Volcano, Papua New Guinea. Rabaul Volcano Work Report Papua New Guinea Dep Miner Policy Geohazards Manag Aust Agency Int Dev Port Moresby Papua New Guinea, 94 p
Jones RH, Stewart RC (1997) A method for determining significant structures in a cloud of earthquakes. J Geophys Res 102:8245–8254
Jonsson S, Zebker H, Amelung F (2005) On trapdoor faulting at Sierra Negra volcano, Galapagos. J Volcanol Geoth Res 144:59–71
Jonsson S (2009) Stress interaction between magma accumulation and trapdoor faulting on Sierra Negra volcano, Galápagos. Tectonophysics 471:36–44
Kabele P, Zak J, Somr M (2017) Finite-element modeling of magma chamber–host rock interactions prior to caldera collapse. Geophys J Int 209:1851–1865
Karlstrom L, Rudolph ML, Manga M (2012) Caldera size modulated by the yield stress within a crystal-rich magma reservoir. Nat Geosci 5:402–405
Kawakami Y, Hoshi H, Yamaguchi Y (2007) Mechanism of caldera collapse and resurgence: observations from the northern part of the Kumano Acidic Rocks, Kii peninsula, southwest Japan. J Volcanol Geoth Res 167:263–281
Kennedy B, Jellinek MA, Stix J (2008) Coupled caldera subsidence and stirring inferred from analogue models. Nat Geosci 1:385–389
Kennedy B, Wilcox J, Stix J (2012) Caldera resurgence during magma replenishment and rejuvenation at Valles and Lake City calderas. Bull Volcanol 74:1833–1847
Kennedy B, Stix J, Hon K, Deering C, Gelman S (2015) Magma storage, differentiation, and interaction at Lake City caldera, Colorado, USA. Geol Soc Am Bull 128:764–776
Kim C-M, Han R, Kim J-S, Sohn YK, Jeong JO, Jepng GY et al (2019) Fault zone processes during caldera collapse: Jangsan Caldera, Korea. J Struct Geol 124:197–210
Koulakov I, Yudistira T, Luehr BG, Wandono, (2009) P, S velocity and Vp/Vs ratio beneath the Toba caldera complex (northern Sumatra) from local earthquake tomography. Geophys J Int 177:1121–1139
Kumagai H, Ohminato T, Nakano M, Ooi M, Kubo A, Inoue H et al (2001) Very-long-period seismic signals and caldera formation at Miyake Island. Japan. Science 293:687. https://doi.org/10.1126/science.1062136
Lagabrielle I, Cormier MH (1999) Formation of large summit troughs along the East Pacific Rise as collapse calderas: an evolutionary model. J Geophys Res 104:12971–12988
Levy S, Bohnenstiehl DR, Sprinkle P, Boettcher MS, Wilcox WSD, Tolstoy M et al (2018) Mechanics of fault reactivation before, during, and after the 2015 eruption of Axial Seamount. Geology 46:447–450
Lindsay JM, de Silva S, Trumbull R, Emmermann R, Wemmer K (2001) La Pacana caldera, N Chile: a re-evaluation of the stratigraphy and volcanology of one of the world's largest resurgent calderas. J Volcanol Geoth Res 106:145–173
Lipman PW (1984) The roots of ash flow calderas in Western North America: windows into the tops of granitic batholiths. J Geophys Res 89:8801–8841
Lipman PW (1997) Subsidence of ash-flow calderas: relation to caldera size and magma-chamber geometry. Bull Volcanol 59:198–218
Lipman PW (2000) Calderas. In: Sigurdsson H, Houghton B, McNutt S, Rymer H, Stix J (eds) The encyclopedia of volcanoes, 1st edn. Elsevier Academic Press, pp 643–662
Liu Y-K, Ruch J, Bathke HV, Jonsson S (2019) Influence of ring faulting in localizing surface deformation at subsiding calderas. Earth Planet Sci Lett 526:115784
Lowenstern JB, Smith RB, Hill DP (2006) Monitoring super-volcanoes: geophysical and geochemical signals at Yellowstone and other large caldera systems. Philos Trans Roy Soc A 364:2055–2072
Mandl G (1988) Mechanics of tectonic faulting: models and basic concepts. Elsevier, Amsterdam, 401 p
Marsh BD (1984) On the mechanics of caldera resurgence. J Geophys Res 89:8245–8251
Martì J, Gudmundsson A (2000) The Las Canadas caldera (Tenerife, Canary Islands): an overlapping collapse caldera generated by magma-chamber migration. J Volcanol Geoth Res 103:161–173
Martì J, Geyer A, Folch A (2009) A genetic classification of collapse calderas based on field studies, and analogue and theoretical modelling. In: Thordarson T, Self S, Larsen G, Rowland SK, Hoskuldsson A (eds) Studies in volcanology: the legacy of George Walker. J Geol Soc Lond Spec Public IAVCEI 2:249–266
Masturyono, McCaffrey R, Wark DA, Roecker SW, Fauzi, Inbrahin G et al (2001) Distribution of magma beneath the Toba caldera complex, north Sumatra, Indonesia, constrained by three dimensional P wave velocities, seismicity, and gravity data. Geochem Geophys Geosyst 2:2000GC000096

Michon L, Massin F, Famin V, Ferrazzini V, Roult G (2011) Basaltic calderas: collapse dynamics, edifice deformation, and variations of magma withdrawal. J Geophys Res 116:B03209. https://doi.org/10.1029/2010JB007636

Mori J, McKee C (1987) Outward-dipping ring-fault structure at Rabaul Caldera as shown by earthquake locations. Science 235:193–195

Munekane H, Oikawa J, Kobayashi T (2016) Mechanisms of step-like tilt changes and very long period seismic signals during the 2000 Miyakejima eruption: insights from kinematic GPS. J Geophys Res 121:2932–2946

Nairn IA, McKee CO, Talai B, Wood CP (1995) Geology and eruptive history of the Rabaul caldera area, Papua New Guinea. J Volcanol Geotherm Res 69:255–284

Neal CA, Brantley SR, Antolik L, Babb JL, Burgess M, Calles K et al (2019) The 2018 rift eruption and summit collapse of Kīlauea Volcano. Science 363:367–374

Newhall CG, Dzurisin D (1988) Historical unrest at large calderas of the world. US Geological Survey Professional Paper 1109 p

Newhall C, Self S, Robock A (2018) Anticipating future Volcanic Explosivity Index (VEI) 7 eruptions and their chilling impacts. Geosphere 14:572–603

Okubo CH, Martel SJ (1998) Pit crater formation on Kilauea volcano, Hawaii. J Volcanol Geoth Res 86:1–18

Orsi G, Gallo G, Zanchi A (1991) Simple shearing block resurgence in caldera depressions. A model from Pantelleria and Ischia. J Volcanol Geoth Res 47:1–11

Orsi G, De Vita S, di Vito M (1996) The restless, resurgent Campi Flegrei nested caldera (Italy): constrains on its evolution and configuration. J Volcanol Geoth Res 74:179–214

Patrick MR, Dietterich HR, Lyons JJ, Diefenbach AK, Parcheta C, Anderson KR et al (2019) Cyclic lava effusion during the 2018 eruption of Kīlauea Volcano. Sci 366: eaay9070

Phillipson G, Sobradelo R, Gottsmann J (2013) Global volcanic unrest in the 21st century: an analysis of the first decade. J Volcanol Geoth Res 264:183–196

Pistolesi M, Isaia R, Marianelli P, Bertagnini A, Fourmentraux C, Albert PG et al (2016) Simultaneous eruptions from multiple vents at Campi Flegrei (Italy) highlight new eruption processes at calderas. Geology 44:487–490

Pritchard ME, Mather TA, McNutt SR, Delgado FJ, Reath K (2019) Thoughts on the criteria to determine the origin of volcanic unrest as magmatic or non-magmatic. Philos Trans Roy Soc 377:20180008

Rivalta E, Corbi F, Passarelli L, Acocella V, Davis T, Di Vito MA et al (2019) Stress inversions to forecast magma pathways and eruptive vent location. Sci Adv 5:eaau9784

Robertson RM, Kilburn CRJ (2016) Deformation regime and long-term precursors to eruption at large calderas: Rabaul, Papua New Guinea. Earth Planet Sci Lett 438:86–94

Roche O, Druitt TH, Merle O (2000) Experimental study of caldera formation. J Geophys Res 105:395–416

Roche O, Druitt TH (2001) Onset of caldera collapse during ignimbrite eruptions. Earth Planet Sci Lett 191:191–202

Roman A, Jaupart C (2014) The impact of a volcanic edifice on intrusive and eruptive activity. Earth Planet Sci Lett 408:1–8

Rougier J, Sparks RSJ, Cashman KV, Brown SK (2018) The global magnitude–frequency relationship for large explosive volcanic eruptions. Earth Planet Sci Lett 482:621–629

Ruch J, Acocella V, Geshi N, Nobile A, Corbi F (2012) Kinematic analysis of vertical collapse on volcanoes using experimental models time series. J Geophys Res 117:B07301. https://doi.org/10.1029/2012JB009229

Rymer H, van Wyk de Vries B, Stix J, Williams-Jones G (1998) Pit crater structure and processes governing persistent activity at Masaya Volcano, Nicaragua. Bull Volc 59:345–355

Self S, Goff F, Gardner JN, Wright JV, Kite WM (1986) Explosive rhyolitic volcanism in the Jemez Mountains: vent locations, caldera development and relation to regional structure. J Geophys Res 91:1779–1798

Seropian G, Stix J (2018) Monitoring and forecasting fault development at actively forming calderas: an experimental study. Geology 46:23–26

Shreve T, Grandin R, Boichu M, Garaebiti E, Moussalam Y, Ballu V et al (2019) From prodigious volcanic degassing to caldera subsidence and quiescence at Ambrym (Vanuatu): the influence of regional tectonics. Sci Rep 9:18868. https://doi.org/10.1038/s41598-019-55141-7

Sigmundsson F (2019) Calderas collapse as magma flows into rifts. Science 366:1200–1201

Simkin T, Howard KA (1970) Caldera Collapse in the Galapagos Islands, 1968. Science 169:429–437

Skilling IP (1993) Incremental caldera collapse of Suswa volcano, Gregory Rift Valley, Kenya. J Geol Soc Lond 150:885–896

Smith RL, Bailey RA (1968) Resurgent cauldrons. Geol Soc Ame Memor 116:613–662

Smith RB, Braile LW (1994) The Yellowstone hotspot. J Volcanol Geoth Res 61:121–187

Smith VC, Isaia R, Pearce NJG (2011) Tephrostratigraphy and glass compositions of post-15 kyr Campi Flegrei eruptions: Implications for eruption history and chronostratigraphic markers. Quatern Sci Rev 30:3638–3660

Solada KE, Reilly BT, Stoner JS, de Silva SL, Mucek AE, Hatfield RG et al (2020) Paleomagnetic observations from lake sediments on Samosir Island, Toba caldera, Indonesia, and its late Pleistocene resurgence. Quatern Res 95:97–112

Stix J, Kobayashi T (2008) Magma dynamics and collapse mechanisms during four historic caldera-forming events. J Geophys Res 113:B09205. https://doi.org/10.1029/2007JB005073

Tibaldi A, Vezzoli L (1998) The space problem of caldera resurgence: an example from Ischia Island, Italy. Geol Rundsch 87:53–66

Trasatti E, Acocella V, Di Vito MA, Del Gaudio C, Weber G, Aquino I et al (2019) Magma degassing as a source of long-term seismicity at volcanoes: the Ischia island (Italy) case. Geophys Res Lett 46. https://doi.org/10.1029/2019GL0853712

Trippanera D, Ruch J, Acocella V, Thordarson T, Urbani S (2018) Interaction between central volcanoes and regional tectonics along divergent plate boundaries: Askja. Iceland. Bull Volcanol 80:1. https://doi.org/10.1007/s00445-017-1179-8

Vazquez JA, Reid MR (2004) Probing the accumulation history of the voluminous Toba Magma. Science 305:991–994

Walker GPL (1984) Downsag calderas, ring faults, caldera sizes, and incremental caldera growth. J Geophys Res 89:8407–8416

Wilcock WSD, Tolstoy M, Waldhauser F, Garcia C, Tan YJ, Bohnenstiehl DR et al (2016) Seismic constraints on caldera dynamics from the 2015 Axial Seamount eruption. Science 354:1395–1399